Diploma Thesis IST-39

Cell–to–Cell Variability in TNF–induced Apoptosis Signalling

Single–Cell and Cell–Population Dynamics

Steffen Borchers

Supervisor: Dr. sc. techn. Eric Bullinger
Dipl.-Biol. Monica Schliemann

National University of Ireland Maynooth
Hamilton Institute
Prof. P. Wellstead

University of Stuttgart
Institute for Cell Biology and Immunology (IZI)
Prof. Dr. P. Scheurich

University of Stuttgart
Institute for System Theory in Engineering (IST)
Prof. Dr.–Ing. F. Allgöwer

31. December 2007

Contents

List of Figures

List of Tables

Introduction

Apoptosis is a process by which the cell commits suicide, e.g. when a cell is damaged. Apoptosis is the most common form of physiologic cell death in multicellular organisms and essentially involved in the development and maintenance of body systems such as the immune response.

The Tumor Necrosis Factor α (TNF) is a representative member of a family of cytokines crucially involved in the coordination of the immune and inflammation response. TNF simultaneously activates pro– and anti–apoptotic signalling pathways in target cells, whereas cell fate depends on numerous factors such as duration and concentration of TNF.

To study and to gain insight in the intricate TNF–induced cellular responses, Schliemann [2006] recently build a single–cell model of the overall TNF–induced apoptosis network in mammalian cells. The model allows to analyse quantitative and dynamical influences of the different pathway components, its predictive power however is limited, since the model lacks a validation phase.

This thesis aims to overcome this bottleneck; the principal hurdle hereby is the TNF–induced apoptosis model being a single–cell model describing the dynamic of apoptosis in an “average” cell. However, there is a variability among individual cells, e.g. cells of the same type exhibit individuality and differences in behaviour if supposed to similar conditions. The single–cell model completely neglects cell variability.

Also, the majority of the available quantitative data is based on bulk–cell techniques measuring average responses combining many cells for analysis, all of which contribute in a different way to the

overall observed behaviour. Therefore, single cell all–or–none or oscillatory behaviour can be masked in the average response. For a predictive understanding of apoptosis process in general and for the adequate evaluation of population–average data in particular, it is important that cell variability is accounted in modeling.

Therefore, a novel cell–population model is derived accounting for heterogeneity of cell populations. The approach considered here is based on a statistical description of cell–to–cell variations, in particular gene expression variability.

This statistical population model allows to calculate and to analyse entire population dynamics and also the statsitics of apoptosis singalling such as cell death distributions. Thereby, the evaluation of population–average data is rendered possible to reestimate models parameters and thus to improve models validity.

The fitted and validated apoptosis single–cell and cell–population models are studied and analysed. The dynamical analysis insights the temporal evolution and transient behaviour of TNF–induced apoptosis. A bifurcation analysis complements this approach with a steady-state view, providing global information of the systems behaviour such as multistationarity and limit cycle oscillations. Also, the key parameters and mechanisms that govern TNF–induced apoptosis dynamics and outputs are identified with the help of parameter sensitivity analysis.

Thesis Structure

This thesis is structured as follows: Chapter 1 provides an introduction of key apoptosis signalling pathways, mechanisms and their mathematical representation. The single–cell model of TNF–induced apoptosis from Schliemann [2006] is outlined and discussed in Section 1.2, and the strategy and the experimental data used to estimate model parameters is presented in Section 1.3. The model changes are summarised in Section 1.4). In Chapter 2, the fitted single–cell model is analysed with respect to models dynamics (Section 2.1), parameter sensitivities (Section 2.2), and bifurcations (Section 2.3).

In Chapter 3, a discourse of cell variability and population heterogeneity is provided and the cell–ensemble population approach is

motivated and derived in Section 3.5. The cell–population model is analysed and validated in Chapter 4. A summarising discussion and an outlook are presented in Chapter 5.

Chapter 1

Mathematical Representation of Apoptosis Signalling

Apoptosis is the most common form of physiologic cell death in multicellular organisms, whereas the balance between cell death and survival is essential. If cells fail to respond to apoptotic signals, cancer may arise. Conversely, disorders such as Parkinson's and Alzheimer's diseases are characterised by excessive apoptotic activity (Haass [1999]).

In the last years, much attention has been paid to identify the complex biochemical networks involved in cell apoptosis. New experimental techniques allow to identify qualitative relationships, and also to measure quantitative time courses of networks components; this provides a basis to build predictive mechanistic models capturing apoptosis signalling.

Signalling for apoptosis occurs through multiple independent pathways that are initiated either from triggering events within the cell (intrinsic) or from outside the cell (extrinsic), for instance, by ligation of death receptors. All apoptosis signalling pathways converge on a common machinery of cell destruction that is activated by caspases (Strasser et al. [2000]). Pro–apoptotic pathways converge to the activation of cell caspases, conversely survival pathways inhibit caspase

activation. Mainly in the last few years, several approaches have been made to describe central apoptosis mechanisms as presented in the next section.

1.1 Introduction to Apoptosis Modelling

A large range of the most important extrinsic signals for apoptosis are received by the Tumor necrosis factor receptor family. Members of the TNF–R family have pleiotropic action (Strasser et al. [2000]). Depending on the cell type and the other signals that the cell receives, these receptors can trigger proliferation, survival, differentiation, or death (Ashkenazi and Dixit [1998], Nagata [1997]). A subfamily of TNF–R family including CD95 (also called Fas or APO–1) and TNF–R1 contain a cytoplasmic region, the death domain, which is essential for activating caspases (Strasser et al. [2000]).

Pro–Apoptotic Signalling Fussenegger et al. [2000] pioneered modeling of apoptosis signalling providing a first attempt to theoretically describe apoptotic signalling including more than 20 reactions. However, this model is based on ad hoc fixed parameters and thus its potential for understanding the regulation of apoptosis is very limited.

An advanced mechanism–based description of caspase–activation is proposed by Eissing et al. [2004], introducing the concept of bistability for caspase activation. The model captures cellular all–or–none behaviour and accounts for the very fast caspase activation observed. Hereby, executioner caspases acts in terms of a positive feedback loop onto initiator caspases, in turn manifesting bifurcating phenotypes, e.g. surviving or dying cells. This model provides a sound description of extrinsically triggered caspase activation.

Gaudet et al. [2005] followed a completely different modeling approach for apoptotic signalling presenting a bottom–up cytokine–signal–response compendium to investigate the regulation of cell fate in cells exposed to combinations of the TNF, EGF, and insulin. The model is derived exclusively from signalling measurements. Whereas the model provided evidence for caspase-cascade regulation via autocrine circuits, the approach rather demonstrated the need for mechanistic models. A mixed mechanistic and black box approach for the caspase activation via CD95 has been considered by Bentele et al. [2004].

Intensive studies on apoptosis revealed a crucial role of mitochondria. It was discovered that these organelles are not only intracellular "power stations" but also a source of pro–apoptotic agents (e.g. cytochrome c) and a target for anti–apoptotic defence (Bcl-2) (Ashkenazi and Dixit [1998]).

Several different models for the intrinsic mitochondria–dependent apoptosis pathways have been suggested. Rehm et al. [2006] focused on the apoptosome–dependent effector caspase activation. Legewie et al. [2006] presented a mathematical model where bistability result from an implicit positive feedback due to competitive inhibition of caspase 3 and 9 by XIAP. Bagci et al. [2006] proposed a model for the mitochondrial pathway based on a cooperativeness mechanism in apoptosome formation and analysed the robustness of bistable behaviour. Eissing et al. [2007] reinvested robustness properties of bistable behaviour comparing three major examples for generating bistability, e.g. cooperativeness, competitive inhibition, and saturation effects. The study demonstrated that none of the three mechanisms appears to be clearly superior regarding the robustness of bistable behaviour with respect to parameter changes (Eissing et al. [2007]).

Anti–Apoptotic Signalling Members of the TNF–R family can also activate the transcriptional regulator NF–κB (Strasser et al. [2000], e.g. TNF–R1. The transcription factor NF–κB is activated via inhibitor κB kinase (IKK) (Micheau and Tschopp [2003]). Importantly, NF–κB promotes transcription of inhibitors of apoptosis (IAP) and FLIP, thus triggering the survival response.

NF–κB activity is strongly regulated. Hoffmann et al. [2002] established a basic IκB–NFκB signalling module based on three IκB–isoforms. The interactions of IKK, IκB isoforms, and NF–κB can be thought of as a negative feedback–containing signal–transduction module (Fig. 1A) that receives signals from pathways emanating from cell-surface receptors (input) and transmits signals to nuclear promoter–bound protein complexes regulating gene expression (output) (Hoffmann et al. [2002]).

This model forms the basis for detailed computational and experimental investigations of the characteristic oscillations in nuclear–cytoplasmic localisation (N–C oscillations) of NF–κB resulting from the negative feedback. Single cell time lapsing experiments have been performed by Nelson et al. [2004], who observed cell–to–cell variations in period and amplitude of these oscillations. The role of IκBϵ isoform has been studied by Kearns et al. [2006], who performed computational studies and knock-out experiments in MEFs. This study provided evidence that IκBϵ has a role in dampening IκBα–mediated oscillations during long-lasting NF–κB activity.

While the Hoffmann model concentrated on the interplay between the three isoforms of NF–κB inhibitory proteins IκBα, IκBβ, and IκBϵ, Lipniacki et al. [2004] proposed a model accounting only for the IκBα isoform and protein A20 inhibitory actions with respect to NF–κB. The model includes two regulatory feedback loops, involving IκBα and A20. Hereby, A20 plays the key role in the dampening of NF–κB oscillations as validated in experimental studies. Furthermore, the model of Lipniacki et al. [2004] accounts for different compartment volumes of the nucleus and cytoplasm.

The previously described approaches mainly focused revealing of the key mechanisms involved in the execution of apoptosis, e.g. positive feedback and bistability of the caspase cascade and negatives feedback involved in the NF–κB response. Of particular practical interest however is the understanding of the complete apoptosis pathways and networks induced by a defined stimulus, e.g. TNF–α, which is a representative member of a family of cytokines involved in immunity and inflammation. Its ligation to TNF–R1 triggers the activation of caspases via the death domain and also induces a survival response via activation of transcription factor NF–κB.

Until now, only very few approaches have been made to establish an overall TNF–induced apoptosis network (Cho et al. [2003], Rangamani and Sirovich [2006]). Cho et al. [2003] presented a model connecting both pathways via inhibitor of apoptosis (IAP), but the model does not account for the fast activation kinetics of executioner caspases as result of positive feedbacks. Based on this model, Rangamani and Sirovich [2006] proposed a TNF–induced overall apoptosis model. Herein, NF-κB transcription activity is simplified to as a delayed reaction; this model does not account for separated nucleus and cytoplasm compartments, and does not include FLIP.

So far, no satisfactory model is published accounting for the close interplay of pro– and anti–apoptotic pathways and fast caspase activation kinetics of TNF–induced apoptosis. In her diploma thesis Schliemann [2006] developed a signal–transduction network for the TNF–induced apoptosis and proposed a preliminary model (Schliemann et al. [2007]); this model forms the basis of this thesis and is presented in the next section.

1.2 TNF–induced Apoptosis Model

The proposed model describes the TNF–α (TNF) induced pro- and anti-apoptotic signalling pathways and their interplay. The single cell model captures the TNF–induced network in the human rhabdomyosarcoma cell line Kym–1, which is characterised by intensive death domain formation and mitochondria-independent caspase-3 activation.

1.2.1 Modules of the Model

The model is build up of three modules, the receptor, the NF–κB pathway and the caspase activation pathway. The models scheme is depicted in Fig. 1.1.

TNF–Reception Extracellular binding of TNF by TNFR immediately induces the formation of a NF–κB activating signalling complex (early complex, C1) by binding of RIP and TRAF2 to the receptor. This complex is internalised building a second signalling complex (late complex, C2), which activates initiator caspases.

Anti–Apoptotic Module This pathway is based on the model proposed by Lipniacki et al. [2004]. The early complex activates the transcription factor NF–κB, which is controlled by two regulatory feedback loops, IκBα and protein A20. NF–κB promotes transcription of inhibitors of apoptosis (IAP) and FLIP. A detailed description of this module is provided in Section 2.1.2.

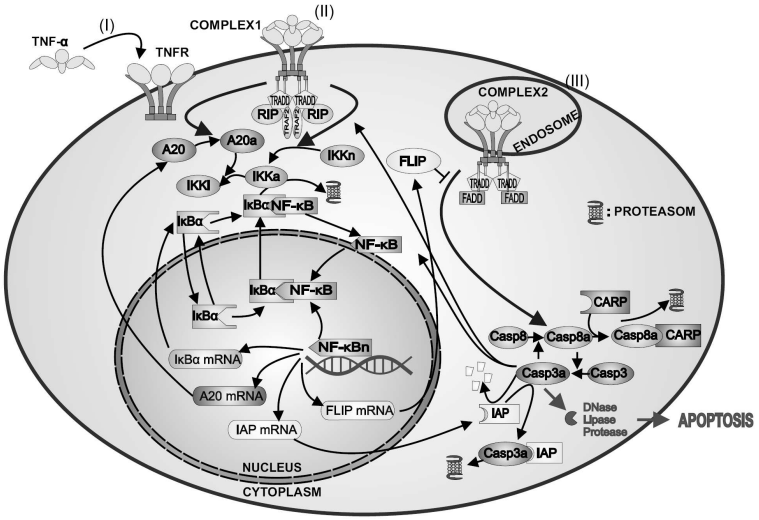

Figure 1.1: Overall scheme of the TNF–induced apoptosis model. Graphic reproduced from Schliemann et al. [2007].

Pro–Apoptotic Module The pro–apoptotic module is based on the caspase cascade proposed by Eissing et al. [2004]. The proapoptotic response is triggered by late complex, activating initiator caspases (subsumed into Caspase 8). The effector caspases are subsumed into Caspase 3 and are activated by active Caspase 8. Hereby, activate Caspase 3 acts in terms of a positive feedback loop onto Procaspase 8, resulting in all–or–none behaviour and very fast caspase activation kinetics. Active Caspase 3 is inhibited by IAP, whereas FLIP inhibits activation of Procaspase 8 by late complex, which couples pro– and anti–apoptotic pathways. A more detailed description of this module is provided in Section 2.1.3.

1.2.2 Mathematical Structure

The model is described as biochemical reaction network consisting of a set of chemical reactions with at most two substrates modelled according to the law of mass action.

Each reaction is of the form

$$A + B \rightleftharpoons C + D$$

resulting in the reaction rate

$$\upsilon = k_+ \cdot [A] \cdot [B] - k_- \cdot [C] \cdot [D] \,.$$

This results in a system of ordinary differential equations including linear and bi-linear terms of the state concentrations, whereas each differential equation is a linear combination of the reaction rates and therefore of the form:

$$\frac{dc_r}{dt} = \sum_{i,j}^{n} k_{i,j} \cdot c_i c_j + \sum_{l}^{n} k_l \cdot c_l + k_o,$$

where $k_{i,j}$, k_l, and k_o denote the constant reaction velocities ($\pm k_+$, $\pm k_-$ or zero).

The overall TNF–induced apoptosis model consists of 42 reaction species and 72 biochemical reactions resulting in about 100 model parameters; the majority of the parameters are taken from the published models of Eissing et al. [2004], Lipniacki et al. [2004] and Hoffmann et al. [2002], whereas the remainder of reaction parameters has been fixed ad hoc.

Qualitatively, this overall model is capable to reproduce several important phenomena of TNF–induced apoptosis. The model accounts for dose–dependency of NF–κB induction, and differences of pulse and continuous TNF–input with respect to executioner caspase activation. However, the model admits structural and quantitative inadequacies and lacks a validation phase.

This thesis aims to overcome this bottlenecks and to re-estimate model parameters. Herefore, the model problems are analyses next, and the set of experimental data is presented and discussed. Based on this data, the strategy for the succeeding model parameter estimation and model validation is outlined.

1.3 Problems and Experimental Data

Simulations studies of the preliminary TNF–induced overall model revealed that the coupling of early Complex 1 with the NF–κB survival pathway is not modeled accurately.

IKK–activation The anti–apoptotic module of the TNF–induced overall model is based on the model proposed by Lipniacki et al. [2004]. This model does not include inhibitor κB kinase (IKK) upstream events, in particular receptor–ligand interactions and signal transduction downstream early Complex 1. Lipniacki et al. [2004] chooses as input for their model a logical variable of the magnitude 1 (μM) in order to capture activation of nonactive IKK if input is "on". The TNF–induced overall model however accounts for the IKK upstream signalling, such that the "accurate" input early C1 is rather dynamic than logic, and in the order of magnitude 1e-3 (μM) , e.g. 1000 times smaller.

Whereas the dynamic of the NF–κB response is qualitatively captured by the preliminary overall model, quantitatively the model predictions of the NF–κB dynamic does not match experimental data.

NF–κB N–C oscillations A central feature of the anti–apoptotic response is the activation of the transcription factor NF–κB. Due to the negative feedbacks involving IκBα and A20, the transcription factor is shuttled repeatedly between the nucleus and cytoplasm. The model predictions are shown in Fig. 1.2; here, the NF–κB N–C oscillations have a period of about 180 min, and are strongly suppressed for almost 250 min for a constant TNF–input. This is not in accord with experimental data, see Section 1.3.1.

CARP An important structural inadequacy concerns the caspase cascade. Recently, the role of CAR–proteins (CARP) has been readdressed (McDonald and El-Deiry [2004], Yang et al. [2007]); the assumed CARP interactions in the caspase cascade are not tenable.

In the model of Eissing et al. [2004], an Caspase 8a inhibitor named BAR/CARP is introduced. It binds to the active Caspase 8, and the bounded complex is degraded. Recent investigations McDonald and El-Deiry [2004], Yang et al. [2007] readdress the role of

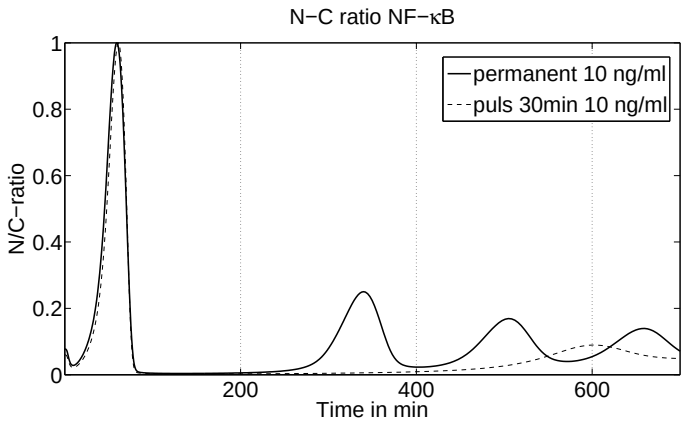

Figure 1.2: Predicted N–C ratio NF–κB of the TNF–induced apoptosis overall model.

CARP. Whereas the specific functions of CARP still remains unclear, experiments indicated that CARP may be involved in the regulation of inactive Caspase 8, but not in the control of its active form, active Caspase 8.

Bid/t–BID The considered TNF–induced apoptosis model encompasses a description of the extrinsic activation of the caspases via late Complex 2. Whereas caspase activation is dominated by this extrinsic pathway in so called Type 1 cells, the caspase–cascade can also be triggered by an intrinsic pathway. Hereby, truncated BID (t–BID) is one important trigger of this intrinsic pathway.

The here considered Kym–1 cells are in the first place Type–1 cells, such that the intrinsic pathway can be neglected in the model. However, Kym–1 cells contain a pool of BID molecules, which are cleaved by active Caspase 8 to truncated BID. For future incorporation of the intrinsic pathway it is desirable to include Bid and the corresponding cleavage reaction.

1.3.1 Experimental Data

The central concern of this thesis is to re-estimate the TNF–induced apoptosis model parameters and to validate the model. For this purpose, quantitative time course data capturing the dynamic of TNF–induced apoptosis is mandatory.

Such quantitative data in general can be obtained studying single cells or cell populations. For example, temporal phenomena such as the NF–κB oscillations in individual cells can be observed by using fluorescence–based imaging assays to quantify protein levels in individual cells at several time points. The majority of the available experimental techniques like Western blotting and EMSA however usually analyse the cell responses from an average of $\sim 10^6$ cells (Sillitoe et al. [2007]).

A principal bottleneck for the purpose of parameter estimation and model validation is that the TNF–induced apoptosis model is a single cell model describing the dynamic of apoptosis in a single, "average" cell. Population–wide measurements however corresponds to population dynamics and cannot be compared directly with single–cell model dynamics, since population dynamics may be biased by the effect of cell variability.

For a predictive understanding of cellular processes in general and for the adequate evaluation of population data in particular, it is important that cell variability is accounted in modeling. Therefore, a population approach will be considered and derived in Chapter 3 allowing to calculate population dynamics and also distributions of apoptosis characteristics such as cell death. Thus, not only single cell but also population–level data can be used for model parameter estimation and model validation. The considered data is presented and discussed in the next section.

Single–Cell Data

Using single–cell time–lapse imaging, Nelson et al. [2004] showed oscillations in NF–κB N–C localisation following cell stimulation with TNF–α in HeLa and SK–N–AS (human S-type neuroblastoma) cells, see Fig. 1.3. The oscillations with a typical period of about 100 minutes continued for up to 20 hours in SK–N–AS cells (Nelson et al. [2004]). In contrast, NF–κB N–C oscillations in HeLa cells were highly damped, but display the same period.

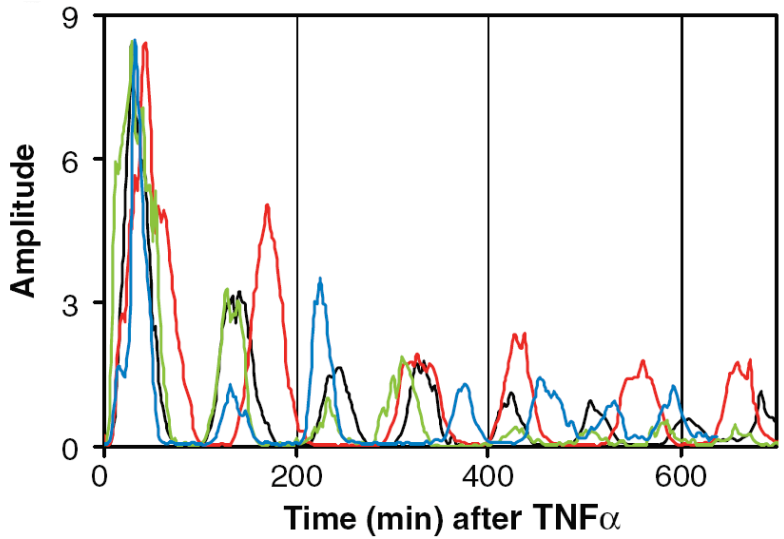

Figure 1.3: Single cell oscillations in NF-κB N–C localisation in SK–N–AS cells (Nelson et al. [2004]). Continuous stimulation with 10 ng/ml TNF-α.

This single cell study provides valuable information about the period of N–C NF–κB oscillations, and also demonstrates significant cell–to–cell variations with respect to NF–κB dynamic, since the individual responses differ in period and amplitudes. Notably, no variations appear in the initial timing of the response (first peak time) (Sillitoe et al. [2007]).

Population–wide Data

Nuclear NF–κB Via the bulk-cell analysis technique EMSA (electrophoretic mobility shift assays), average levels of nuclear NF–κB have been monitored Schliemann [2007] for a Kym–1 cell population, see Fig. 1.4. High time–resoluting data is available for low (0.3 ng/ml,

see Fig. 1.4(a)) and high (10 ng/ml, see Fig. 1.4(b)) TNF–inputs.

From the data, some general information can be extracted; the timing of the initial response is about 40 min. Nuclear NF–κB activity is terminated for low–dose pulse input after about 150 min, in contrast to constant and high–dose pulse input, where NF–κB activity is maintained. Also, the timing and amplitude of nuclear NF–κB is dose dependent (see Fig. 1.4(c)), at least for a range of 0.01 ng/ml $\leq$ TNF $\leq$ 3 ng/ml.

Cytotoxicity The population death distributions with respect to different TNF–inputs have been measured in cytotoxicity assays (see Fig. 1.5) considering Kym-1 cells treated with serial dilutions of TNF–α (Schliemann et al. [2007]). The data clearly indicate TNF–input dependency. For low concentrations ($\leq$ 0.3 ng/ml) of TNF–α, neither a continuous (Fig. 1.5(a)) nor a pulse (Fig. 1.5(b)) treatment leads to cell death, while for very high concentrations ($\geq$ 30 ng/ml) the cells undergo apoptosis; nevertheless cells survive even for very high TNF–concentrations. For intermediate concentrations, cells are sensitive with respect to the duration of the TNF–input. .

Further Considered Data The data of levels of nuclear NF–κB as well as cytotoxicity assays are consistent in terms of being obtained from the same cell type (Kym–1 cells). Since the model preferably aims to capture TNF–induced apoptosis in this cells, this data is favoured. Nevertheless, the data obtained by Nelson et al. [2004] in MEFs is also taken into consideration, in particular levels of cytoplasmic IκBα, A20 and IκBα mRNA transcripts, and IKK and IKK catalytic activity. Unfortunately, the data is not quantified.

In summary, the following trends can be extracted from the experimental data; these specifications will enter the succeeding model parameter adaptation in the next chapter.

- N–C NF–κB oscillations: period $\sim$100 min
- Initial timing of nuclear NF-κB about 40 minutes for intermediate and high TNF–inputs
- Saturation of nuclear NF–κB amplitude for high TNF–inputs

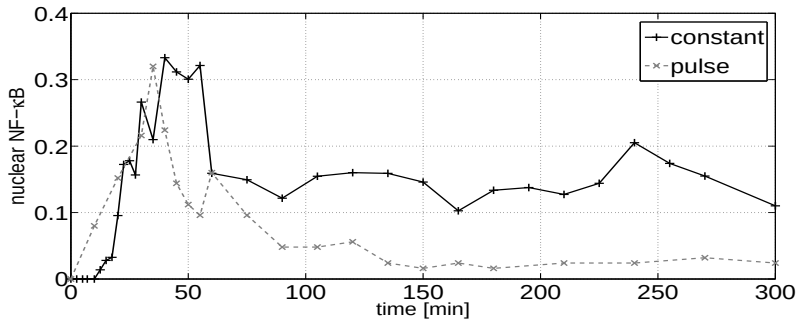

(a) Low TNF–dose 0.3 ng/ml.

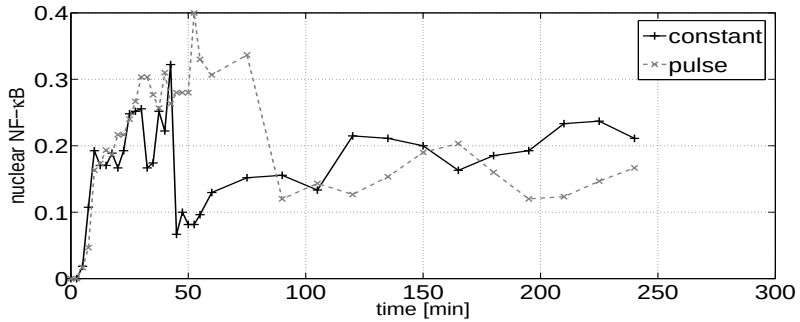

(b) High TNF–dose 10 ng/ml.

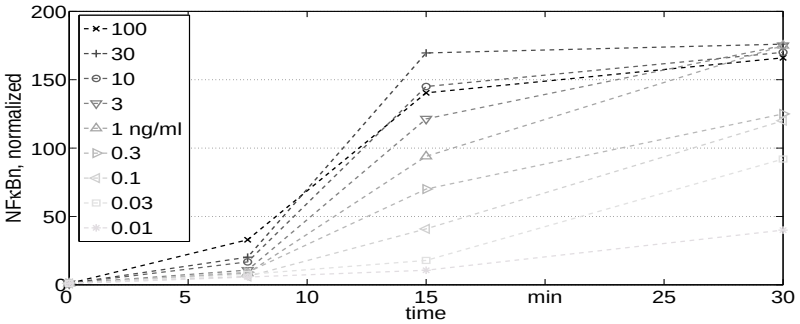

(c) EMSA start dynamic.

Figure 1.4: EMSA data. Schliemann [2007], IZI Stuttgart, unpublished data.

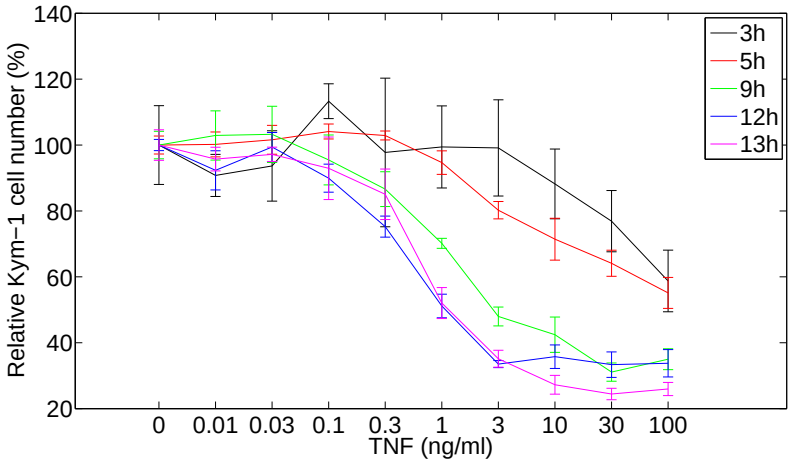

(a) Constant TNF–input.

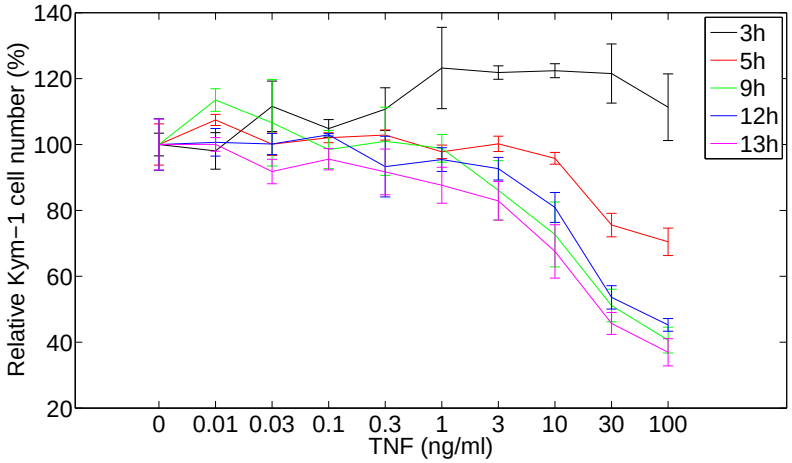

(b) 30 min pulse TNF–input.

Figure 1.5: Cytotoxicity data. Schliemann [2007], IZI Stuttgart, unpublished data.

- Termination of nuclear NF–κB activity for low pulse inputs, maintained activity for constant TNF–inputs
- Surviving cells even for high TNF–inputs (resistance)
- TNF–dose dependency: NF–κB and cell viability
- Fast caspase activation

1.4 Model Changes

This section explains the difference between the model of Schliemann [2006] and the model proposed here. The changes encompass some structural modifications of the caspase–cascade and model parameter changes. The parameters are reestimated with the help of the population model in Chapter 3.

In particular, the molecule CARP and its interactions are removed as explained in Section 1.4.1. To provide an interface to the intrinsic pathway of apoptosis, the protein BID and the corresponding interactions with active Caspase 8 are introduced in Section 1.4.2. The most important model parameters changes are discussed in 1.4.3 and summarised in the Tables 5.1–5.3 in the Appendix.

1.4.1 Removal of CARP–Interactions

The caspase cascade model of Eissing et al. [2004] considers CARP (also known as BAR) protein to bind and inhibit active Caspase 8 similar to the interactions of IAP and active Caspase 3. The molecule is introduced in order to limit the amount of free active caspase 8 and thus to realise fast caspase activation kinetics according to parameter values from literature.

The role of CARP however has been readdressed (McDonald and El-Deiry [2004], Yang et al. [2007]). CARP's mediate a pro–apoptotic effect acting as E3 ligases for p53 (Yang et al. [2007]) rather than controlling active caspases (McDonald and El-Deiry [2004]). Therefore, the inhibitory role of CARP's is not tenable; hence, an inhibitor for active Caspase 8 is not further considered in the here proposed model.

Nevertheless, removal of CARP's entails a slew of changes of the model parameters, e.g. a higher degradation rate of active Caspase

8 and decreased activation of Caspase 3 by active Caspase 8; the changes are summarised in Table 5.3 in the Appendix.

The amount of free active Caspase 8 however is also altered considering additional cleavage activities of active Caspase 8 such as cleavage of Bid to t–Bid (see next section).

1.4.2 Uptake of BID–Interactions

The considered TNF–induced apoptosis model encompasses a description of the extrinsic activation of the caspases via late Complex 2. Whereas caspase activation is dominated by this extrinsic pathway in so called Type 1 cells, the caspase–cascade can also be triggered by an intrinsic pathway. Hereby, truncated Bid (t–Bid) is one important trigger of this intrinsic pathway.

The here considered Kym–1 cells are in the first place Type–1 cells, such that the intrinsic pathway is not relevant. However, Kym–1 cells still contain a pool of Bid molecules, which are cleaved by active Caspase 8 to truncated BID. The BID protein and this cleavage reaction are taken up in the model considering mass action principles, but not downstream signalling of t–Bid. The considered reaction scheme is depicted in Fig. 1.6.

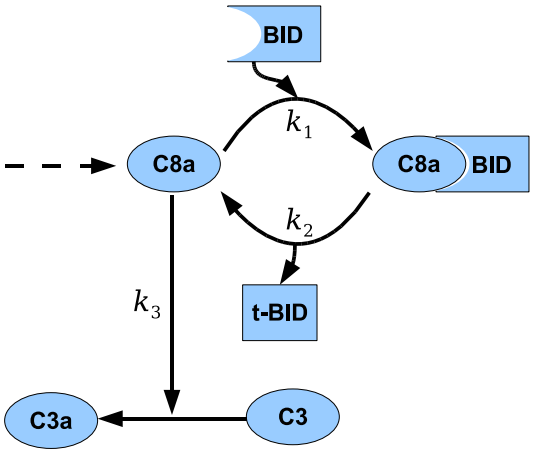

Figure 1.6: BID reaction scheme.

The turnover of BID is described by

$$0 \underset{k_-}{\overset{k_+}{\rightleftharpoons}} \text{BID},$$

whereas k_+ denotes the (constant) expression and k_- the (constant) degradation rate of BID. Since no biochemical data is available to estimate the corresponding parameter values, k_+ is assumed to be in the same order of magnitude as expression of IAP, and the degradation rate k_- is fitted concerning the cytotoxcicity data, see Fig. 1.5.

Active Caspase 8 transiently associates with BID forming the complex C8a∼BID with the association rate k_1, and cleaves BID to truncated BID with the cleavage rate k_2. The association rate k_1 and cleavage–rate k_2 are considered as high as active Caspase 8 cleaves Procaspase 3 (k_3). Truncated BID is assumed to degrade constantly with k_-^{tBID}. Table 1.1 summarise the corresponding kinetics.

Reaction	**symbol**	**value μM**
0⇌BID	k_+	2.8e-5
	k_-	1.6e-5
C8a+BID→C8a∼BID	k_1	0.04
C8a∼BID→C8a+tBID	k_2	0.04
t–BID→0	k_-^{tBID}	5e-5

Table 1.1: Cleavage of BID to t–BID.

1.4.3 Model Parameter Changes

Here, an overview over the most important model parameter changes is provided.

Activation of A20 Active A20 inactivates active IKK, e.g.

$$\text{IKKa} + \text{A20a} \rightarrow \text{IKKi} + \text{A20a}.$$

Expression of A20 is induced by NF–κB, and A20 is assumed to play an important role in the dampening of NF–κB oscillations. To

account for this regulatory function, the activation velocity of A20 by early Complex 1, e.g.

$$\text{A20} + \text{C1} \rightarrow \text{C1} + \text{A20a},$$

is raised by factor 10, now at 2.5 $(\mu\text{Ms})^{-1}$.

Activation of IKK The nonactive inhibitor κB kinase (IKKn) is activated by early Complex 1 (C1), e.g.

$$\text{IKKn} + \text{C1} \rightarrow \text{IKKa} + \text{C1}. \tag{1.1}$$

This activation mechanism is based on Lipniacki et al. [2004], where C1 was assumed to be a logical input variable, e.g. 0 or 1 [μM], since signalling upstream C1 has not been considered. The TNF–induced apoptosis model accounts for this upstream signalling, such that the actual level of C1 is dynamic and in the order of 1e-3 [μM]. As a result, only a small amount of IKKn is activated in the model of Schliemann [2006], see Fig. 1.7; even for high TNF–inputs, less than 1 percent of IKKn are activated, which is biologically not reasonable.

The activation velocity of Reaction 1.1 is therefore raised by factor 300. This in turn results in high levels of active IKK (not shown here), which is compensated by accelerating the inactivation of active IKK, e.g.

$$\text{IKKa} \rightarrow \text{IKKi},$$

by factor 15 (now at 2.25e-2 s^{-1}).

To achieve an NF–κB activity for constant TNF–inputs, the dissociation rate of the complex formed by IKKa and IκB$\alpha\sim$NF–κB, e.g.

$$\text{IKKa}\sim\text{I}\kappa\text{Ba}\sim\text{NF}\text{–}\kappa\text{B} \rightarrow \text{IKKa} + \text{NF}\text{–}\kappa\text{B}$$

is decreased by factor 40 (now at 2.5e-3 s^{-1}). The changes are summarised in Table 5.2 in the Appendix.

Ratio of cytoplasm to nucleus The ratio of cytoplasm to nucleus of the model has been changed to 2.5, whereas Lipniacki et al. [2004] assumes a ratio of 5 is assumed. The ratio of 2.5 approximately accounts for Kym–1 cells.

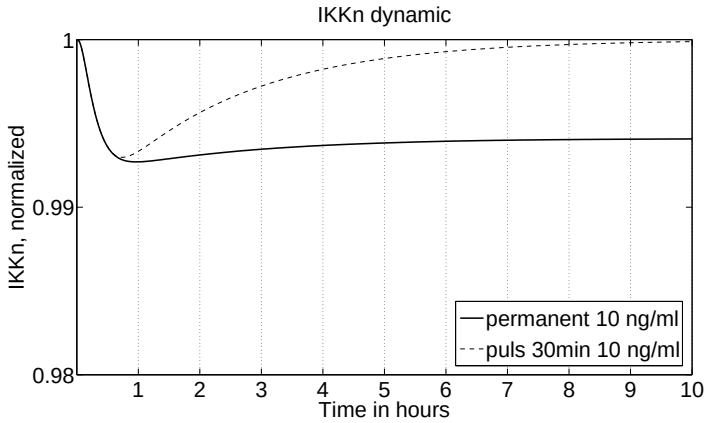

Figure 1.7: IKKn dynamic for high TNF–input (10 ng/ml) in the model of Schliemann [2006]. The concentration of IKKn is normalised to the resting steady state concentration.

Transcription of IAP mRNA The transcription rate of IAP mRNA by nuclear NF–κB, e.g.

$$\text{NF}\text{–}\kappa\text{Bn} \rightarrow \text{IAPt} + \text{NF}\text{–}\kappa\text{Bn}$$

is reduced by factor 10, whereas the basal expression rate of IAP, e.g.

$$0 \rightarrow \text{IAP}$$

is raised by factor 2.7. The balance of both, basal and NF–κB–induced production of IAP, influences the cell death distributions for pulse and constant TNF–inputs. High NF–κB–induced IAP expression along with higher survival rates for constant TNF–inputs than (same amplitude) pulse inputs, which is biologically not reasonable.

Degradation of active Caspase 8 The removal of CARP as regulatory molecule for active Caspase 8 entails a slew of changes. To achieve stability of the unstimulated steady state, degradation of active Caspase 8, e.g.

$$\text{C8a} \rightarrow 0,$$

is raised by factor 8, and the activation of Procaspase 8 by late Complex 2, e.g.

$$C8 + C2 \rightarrow C8a + C2,$$

is reduced by factor 4. The changes are summarised in Table 5.3.

The previouly described parameter changes can not be considered as an unique solution of the estimation problem, e.g. the qualitative and quantitative accordance with the experimental data can also be achieved considering other parameters changes. The here fitted parameters are unsure parameters, e.g. have not yet been determined experimentally.

1.5 Summary

TNF–α is a representative member of a family of cytokines involved in immunity and inammation. Its ligation to TNF–R1 induces controversial cellular responses, in particular the activation of caspases and a survival response. Aiming a better understanding of TNF–induced apoptosis, a mathematical model of the underlying signalling network has recently been modeled by Schliemann [2006]. The model accounts for the close interplay of pro– and anti–apoptotic pathways in Kym–1 cells.

Qualitatively, this overall model captures the most important phenomena related to TNF–induced apoptosis. However, the model admits some inadequacies that need to be corrected and lacks a validation phase.

The central issue of this thesis is to re-estimate the TNF–induced apoptosis model parameters and to validate the model. Herefore, precise quantitative data is available, though mainly from bulk–cell analysis techniques. Since the TNF–induced overall model is a single cell model, a population approach will be considered and derived in Chapter 3. This allows to evaluate the data obtained by cytotoxicity assays and EMSA adequately for the purpose of parameter identication and model validation.

The TNF–induced model developed by Schliemann [2006] is structurally modified and the model parameters have been changed according to the experimental data. The structural modifications concern

the caspase cascade; CARP interactions are depleted from the new model proposed here, since no evidence is provided for a inhibitory molecule of active Caspase 8. Furthermore, the BID protein and the related cleavage reactions by active Caspase 8 are taken up in the new model. This will allow to interface the intrinsic apoptosis pathway in future work.

The model parameters are reestimated and fitted according to EMSA and cytotoxicity data. The resulting model accomplishes the specifications outlined in Chapter 1, and is validated considering the experimental data as shown in Chapter 4. The complete lists of the reactions, parameters, and initial values of the fitted apoptosis model proposed here are provided in the appendix. This model forms the basis for the following analysis.

Chapter 2

Analysis of the Apoptosis Single–Cell Model

Quantitative modeling in systems biology is of great advantage for the purpose of a better understanding of the regarded process. Insights into the dynamic behaviour of biological networks can be obtained from mathematical analysis; herfore, several powerful analysis approaches are applicable.

Simulation is essential to study the temporal evolution and transient behaviour of the system. A bifurcation analysis complements this approach with a steady-state view, providing global information of systems behaviour such as multistationarity and limit cycle oscillations along large parameter variations. A sensitivity analysis helps to identify those parameters that govern system dynamics and outputs.

The analysis performed in the chapter yields to insight TNF–induced apoptosis signalling. The changed and fitted model forms the basis for the following single–cell level analysis. A dynamical analysis is performed in Section 2.1 providing insight in the temporal and transient features of TNF–induced apoptosis. Then, a local parameter sensitivity analysis is performed in Section 2.2 identifying the most sensitive components and mechanisms of apoptosis signalling. The bifurcation analysis provided in Section 2.3 addresses the issue of bistability of the caspase cascade and is used to investigate the oscillatory feature of the NF–κB signalling for large variations of the most sensitive parameters.

2.1 Dynamical Analysis

Dynamical analysis is essential to insight the temporal behaviour of a dynamical system. Hereby, the system is simulated and the system trajectories are studied. This provides insights into the kinetics of the underlying signalling process and elucidates transient mechanisms such as all–or–none switching or oscillatory behaviour of the system away from equilibrium.

In this section, the time evolution of the new TNF–induced apoptosis model is studied. The signal flow downstream the TNF–receptor is analysed concerning different TNF–inputs;the induction of the anti–apoptotic response via activation of the early Complex 1 is studied in Section 2.1.2, and the proapoptotic response downstream the late Complex 2 in Section 2.1.3. Their interplay is analysed in Section 2.1.4.

2.1.1 TNF Downstream Signalling

Binding of TNF–ligand to its cell surface receptor immediately induces the formation of the early Complex 1 (see Fig. 2.1) via docking

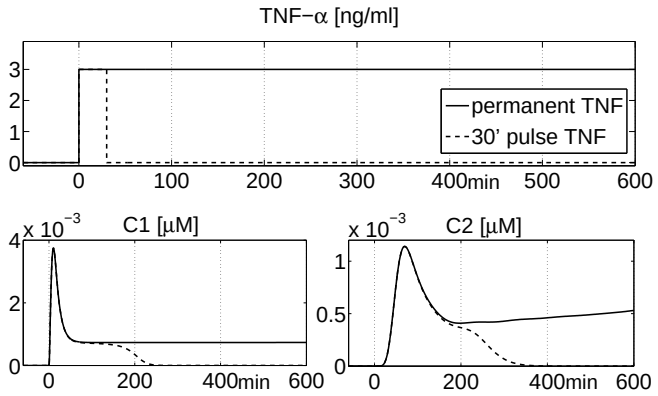

Figure 2.1: TNF–induced immediate formation of the early Complex 1 and delayed formation of late Complex 2.

of adaptor proteins such as RIP to the intracellular domain of the TNF–receptor (death domain). The early Complex 1 then is internalised, modeled by a chain of delaying reactions, and modified leading to the formation of the late Complex 2. The formation of late Complex 2 is delayed by by about one hour.

The early Complex 1 triggers the anti–apoptotic response, whereas late Complex 2 triggers the activation of effector caspases as explained next.

2.1.2 Downstream C1 Signalling

The anti–apoptotic cellular response is induced by activation of the IκB kinase (IKK) by early Complex 1, see Fig. 2.2. Hereby, the nonactive IκB kinase (IKKn) is activated (IKKa).

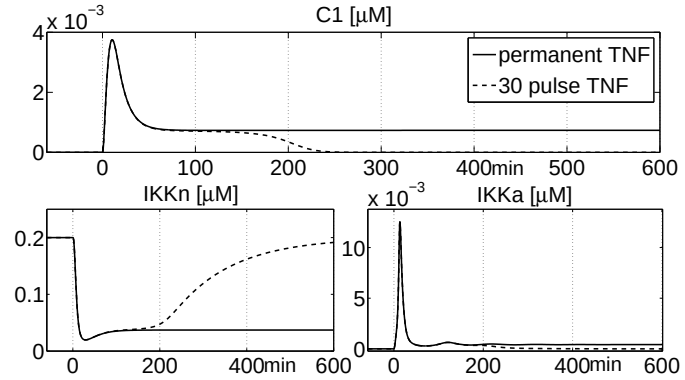

Figure 2.2: Downstream C1 signalling. Activation of the nonactive IκB kinase is induced by early Complex 1.

NF–κB Activation and N–C Oscillations The interactions of IKK, IκBα, and NF–κB can can be described by a negative feedback containing interaction module (Hoffmann et al. [2002]), see Fig. 2.3.

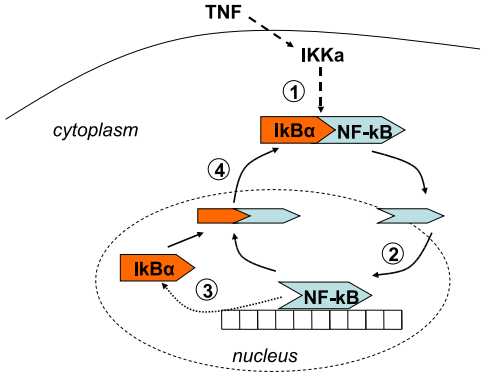

Figure 2.3: NF–κ regulatory scheme.

In the resting state, NF–κB is retented in the cytoplasm within the complex IκBα∼NF–κB. The active IκB kinase phosphorylates IκBα, leading to its ubiquitination and proteolysis. IκBα degradation liberates NF–κB from the complex ①, which is subsequently translocated to the nucleus ②; NF–κB binds DNA inducing transcription of several genes, so its inhibitor IκBα ③. The synthesised IκBα binds to nuclear NF–κB and induces the export of the complex ④. Persistent levels of active IKK (constant TNF–input) lead to damped oscillations of NF–κB and IκBα.

Fig. 2.4 shows the time evolution of the components involved in the negative feedback. Nuclear NF–κB and IκBα admit damped thus transient but antiphasic oscillations with a period of about 100 min, which is in accord with the single cell experiments of Nelson et al. [2004] and Sillitoe et al. [2007].

For a continuous TNF–input, a constant level of nuclear NF–κB is reached after about 6 hours, whereas for the 30 min. pulse input the level of nuclear NFB decreases to zero after about 240 minutes. This holds only for high pulse TNFlevels (> 1 ng/ml), otherwise no second peak occurs (data not shown).

Nuclear NF–κB is liberated an translocated rapidly; the level of nuclear NF–κB peaks 50 min after the TNF–input is applied, which is in accord with the EMSA data (Section 1.3.1). Hereby, the activation of NF–κB is the faster the higher the TNF–dose (data not shown).

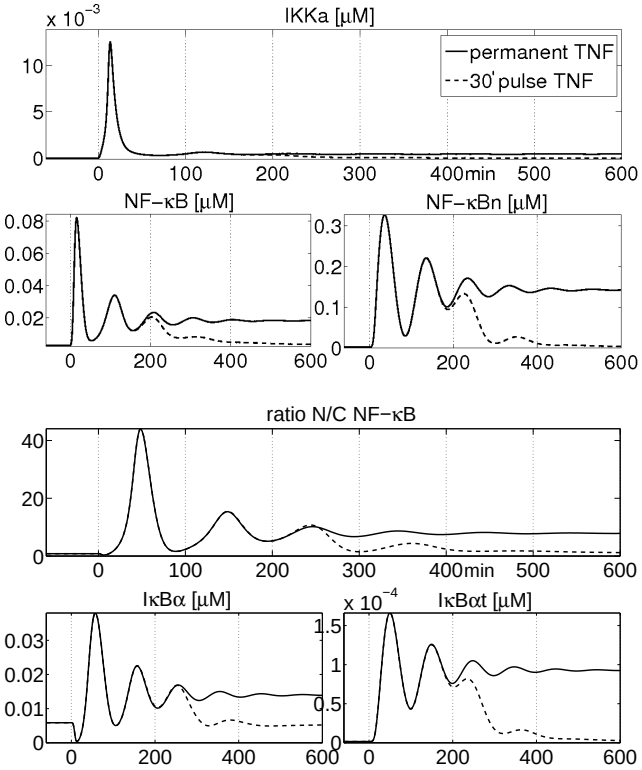

Figure 2.4: Nucleus–cytoplasmic oscillations of NF-κB and IκBα. Ratio N/C NF-κB normalised to basal level.

NF-κB Transcription Activity Nuclear NF-κB promotes transcription of several compounds involved in TNF–induced apoptosis signalling, see Fig. 2.5. Nuclear NF–κB promotes transcription of its own inhibitors IκBα and A20 mRNA, and caspase inhibitors IAP and FLIP.

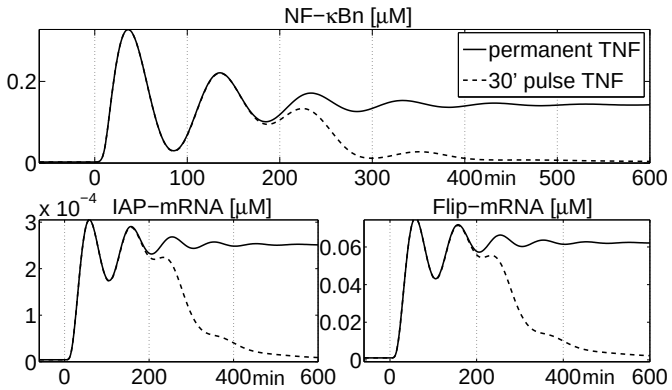

Figure 2.5: Nuclear NF–κB promotes transcription of caspase inhibitors IAP mRNA and FLIP mRNA.

2.1.3 Downstream C2 Signalling

Caspases Apoptosis is initiated and executed by aspartate directed cysteine proteases, the caspases. Caspases are produced as proenzymes and are activated upon pro–apoptotic signals.

The initiator Caspase 8 is activated by late Complex 2, see Fig. 2.6. Active Caspase 8 in turn cleaves Procaspase 3, an executioner caspase. Activated Caspase 3 acts in terms of a positive feedback loop onto Procaspase 8. Due to this positive feedback, Caspase 3 is activated in an all–or–none fashion, and the activation occurs very rapid within 30 min. if the pro–apoptotic signal is strong enough. Note that for pulse TNF–input (dashed lines), Caspase 3 is not fully activated, e.g. the cell survives. Cell death along with full activation of Caspase 3 as for the constant TNF–input.

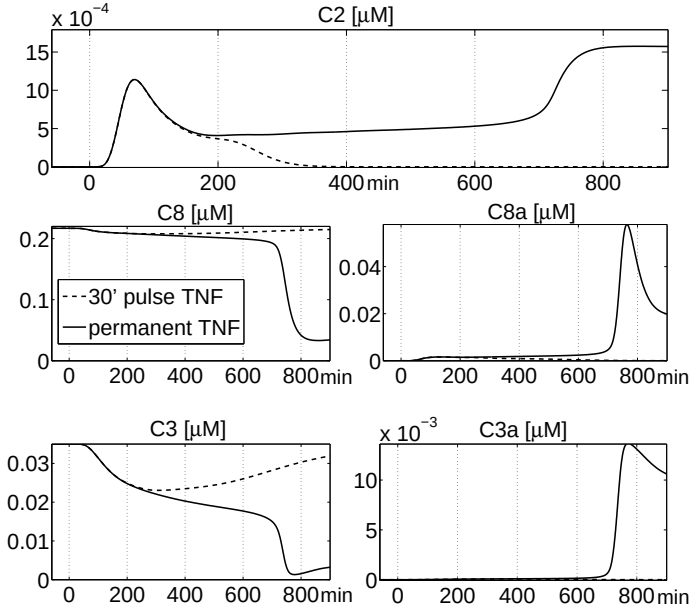

Figure 2.6: Triggering of the caspase cascade by late complex C2. Activation of Caspase 3 occurs for constant TNF–input, but not for pulse input.

Bid Active Caspase 8 not only cleaves Procaspase 3, but also cleaves Bid to t-Bid. The dynamic of Bid truncation is presented in Figure 2.7.

t–Bid is a hallmark in the induction of the mitochondrial pathway of apoptosis, as t–Bid leads to the release of cytochrome C and Smac/DIABLO. The here considered Kym–1 cells are at first place Type I cells, such that the mitochondrial pathway is neglected. However, Kym–1 cells nevertheless contain a pool of BID molecules, which are cleaved by active Caspase 8 to t–Bid. Since active Caspase 8 bounds to t–BID, its free amount is transiently limited and thus full activation of the caspases is delayed.

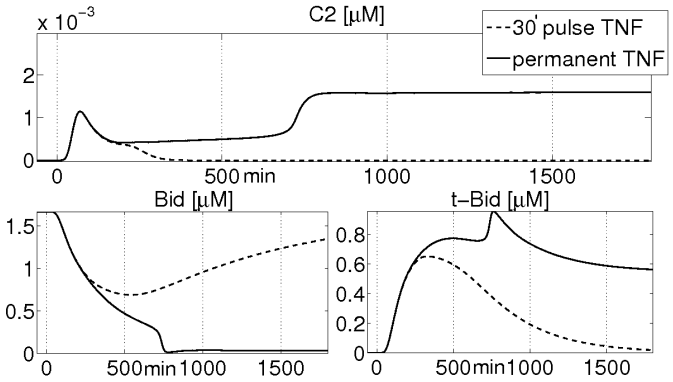

Figure 2.7: Truncation of BID to t-BID by active Caspase 8..

In summary, TNF induces two concurring pathways, e.g. pro–apoptotic via activation of caspase cascade and anti–apoptotic via NF–κB and subsequent production of caspase inhibitors IAP and FLIP. A TNF–concentration of 3 ng/ml induces full activation of Caspase 3 and therefore cell death for the continuous TNF input, whereas the cell survives for the 30 minutes pulse TNF input. In this case, the survival response superiors, e.g. prevents the activation of the caspases. To understand this bifurcating behaviour, the interplay of survival and death–inducing cell response are analysed in the next section.

2.1.4 Interplay of Pro– and Antiapoptotic Responses

The caspase cascade is coupled to the anti–apoptotic response via NF–κB–induced expression of apoptosis inhibitors IAP and FLIP. FLIP binds with late Complex 2 to FLIP∼C2, promoting its degradation. Thus, FLIPs diminish the concentration of free C2 (see Fig. 2.8), in turn lowering the pro–apoptotic signal.

To study the impact of FLIP and the timing of pro- and antiapoptotic responses, the interaction of FLIP with C2 are knocked–out and compared with the actual dynamic, see Fig. 2.8.

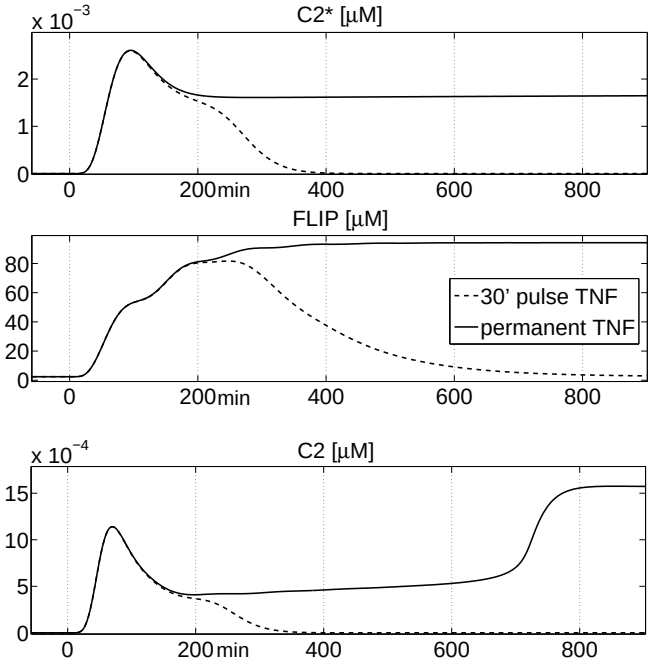

Figure 2.8: Timing of pro– and antiapoptotic cell responses. TOP: late Complex 2 dynamic with knocked–out C2–FLIP interactions. CENTER: FLIP dynamic with knocked–out C2–FLIP interactions. BOTTOM: Actual C2 dynamic.

The early Complex C1 is formed immediately after TNF stimulation, inducing NF-κB to be activated within 50 minutes. Nuclear NF–κB promotes the transcription FLIP. Since the formation of C2 is delayed by about one hour, cell anti–apoptotic response is in time. A sufficient amount of additional FLIP is provided preventing cell death at 3 ng/ml 30 min. pulse stimulation, but not in the continuous stimulation case, since Complex 2 is continuously delivered. Cell fate therefor not only depends on the TNF–input, but also on the timing of pro– and anti–apoptotic responses.

2.1.5 Summary Dynamical Analysis

TNF–induced apoptosis signalling is double–edged. TNF–stimulation leads to the formation of the early Complex 1, which forms the pedestal for two concurring apoptosis pathways. The early Complex 1 triggers the anti–apoptotic response, whereas late Complex 2 triggers the activation of caspase cascade.

The early Complex 1 rapidly activates IκB kinase leading to dissociation of the complex IκB$\alpha\sim$NF–κB and subsequently to the translocation of the NF–κB to the nucleus. Liberation and translocation occur rapidly; the level of nuclear NF–κB peaks 50 min after the TNF–input is applied.

In the nucleus, NF–κB promotes transcription of several genes, among them its own inhibitor IκBα, which establishes a negative feedback driving transient oscillations of NF–κB, whereas a level of NF–κB is maintained if TNF–input persists. These oscillations are dampedand admit a period of about 100 min, which is in accord with the single cell experiments of Nelson et al. [2004] and Sillitoe et al. [2007].

The formation of late Complex 2 is delayed by about one hour. Late Complex 2 activates initiator Caspase 8, thus triggering the caspase cascade. Hereby, active Caspase 3 acts in terms of a positive feedback loop onto Procaspase 8 resulting in an all–or none behaviour, e.g. the cell survives (no activation of executioner Caspases 3) or the cell dies (full activation of Caspase 3). If the activation is triggered, caspases are fasty activated within 30 minutes.

The caspase cascade is coupled to the anti–apoptotic response via apoptosis inhibitors IAP and FLIP. Hereby, FLIP diminishes the concentration of free C2 thus reducing the strength of cascade triggering signal. Delayed induction of the pro–apoptotic pathway provides the cell time to produce additional inhibitors. Cell fate not only depends on the TNF–input, but also on the timing of pro– and anti–apoptotic responses.

2.2 Sensitivity Analysis

Sensitivity analysis is an important tool to study the dependence of a system on its parameters, and to analyse how sensitive the system is with respect to the model parameters. The study of sensitivities helps to identify those parameters that govern system dynamics and outputs even in larger networks such as the TNF–induced apoptosis. Sensitivity coefficients, which are the partial derivatives of the model states with respect to the model parameters, play an important role in experimental design, parameter estimation, uncertainty analysis, model discrimination and reduction, etc. for biological systems (Yue et al. [2006]).

In this section, the local parameter sensitivities of the TNF–apoptosis model are studied, e.g the influence of small parameter perturbations. In Subsection 2.2.1, the overall maximal sensitivity coefficients for the model states are presented for two different TNF–inputs. This sensitivity coefficients are obtained by differentiation of the analytical solution of the ODE model considering a maximum norm, whereas the sensitivity coefficients for the nonanalytic apoptosis characteristics presented in Subsection 2.2.2 are obtained numerically. The results for a particular class of model parameters, the gene expression rates, are summarised in Subsection 2.2.3. A summary is provided in Subsection 2.2.4.

For all the calculations relating to dynamic sensitivities and other sensitivities, the dynamic time length is 10 hours, since this timeframe is biologically relevant and suffices for TNF–induced apoptosis in Kym–1 cells; the amplitude of the TNF–input is 10 ng/ml.

2.2.1 Sensitivity Coefficients

TNF–induced apoptosis is described as biochemical reaction network consisting of a set of chemical reactions with at most two substrates modelled according to the law of mass action.

Each reaction is of the form

$$A + B \rightleftharpoons C + D$$

resulting in the reaction rate

$$\upsilon = k_+ \cdot [A] \cdot [B] - k_- \cdot [C] \cdot [D]\,.$$

This results in a system of differential equations including linear and bilinear terms of the state concentrations, which can be written in a very compact form:

$$\dot{\underline{x}}(t) = \underline{f}\big(\underline{x}(t), \underline{\theta}\big) + u(t), \;\; \underline{x}(t) \in \mathbb{R}^n_+, \; t \geq 0 \;, \underline{\theta} \in \mathbb{R}^m_+$$

with the initial conditions

$$\underline{x}(0) = \underline{x}_o, \; \underline{x}_o \in \mathbb{R}^n_+.$$

Hereby, $\underline{x}(t)$ denotes the species concentrations, $u(t)$ the (non–negative) TNF–input, and $\underline{\theta}$ the reaction parameters $[k_+, k_-]$.

Denoting x_i as the ith state and θ_j as the jth parameter in $\underline{\theta}$, the dynamic state sensitivity coefficient is given by the derivation of the model state with respect to the model parameter,

$$S^{x_i}_{\theta_j}(t) = \frac{\partial x_i(t)}{\partial \theta_j} =: S^i_j(t).$$

To obtain the state sensitivities, the sensitivity differential equation system has to be solved. This differential equation system is derived as follows:
Since

$$\dot{\underline{x}} = \frac{d\underline{x}}{dt} = \underline{f}(\underline{x}, \underline{\theta}) \tag{2.1}$$

it holds

$$\frac{\partial}{\partial \underline{\theta}}\left(\frac{d\underline{x}}{dt}\right) = \frac{\partial}{\partial \underline{\theta}}\Big(\underline{f}(\underline{x}, \underline{\theta})\Big).$$

With

$$\frac{\partial}{\partial \underline{\theta}}\left(\frac{d\underline{x}}{dt}\right) = \frac{d}{dt}\left(\frac{\partial \underline{x}}{\partial \underline{\theta}}\right), \;\; \frac{\partial}{\partial \underline{\theta}}\Big(\underline{f}(\underline{x}, \underline{\theta})\Big) = \frac{\partial \underline{f}}{\partial \underline{x}} \cdot \frac{\partial \underline{x}}{\partial \underline{\theta}} + \frac{\partial \underline{f}}{\partial \underline{\theta}} \cdot 1,$$

whereas

$$\frac{\partial \underline{x}}{\partial \underline{\theta}} =: \underline{S}(t)$$

denotes the sensitivity matrix and

$$\frac{\partial \underline{f}}{\partial \underline{x}} =: \underline{J}$$

the Jacobian matrix. Hence it follows

$$\dot{\underline{S}}(t) = \underline{J} \cdot \underline{S}(t) + \frac{\partial \underline{f}}{\partial \underline{\theta}}, \tag{2.2}$$

whereas the initial conditions of $\underline{S}(t = 0)$ can be obtained by differentiation of the initial condition of $\underline{x}_o$ as follows (Yue et al. [2006]):

$$S^i_j(t = 0) = \delta(\theta_j - x^o_i).$$

Hereby, δ denotes the Kronecker delta function.

Solving the differential equation systems 2.1 and 2.2 yields the sensitivity coefficients, whereas $S^i_j(t)$ is the (i, j)th entry of the sensitivity matrix $\underline{S}(t)$. The sensitivity coefficients vary over time and are elements of $\mathcal{L}_2[0, 10h]$–space, e.g. it holds

$$\|S^i_j(t)\|_2 = \sqrt{\int_0^{10h} |S^i_j(\tau)|^2 d\tau} < \infty.$$

For the purpose of analysis, the following relative sensitivities are used instead of $S^i_j(t)$ allowing direct comparison of responses at different states or across different parameters:

$$\overline{S}^i_j(t) = \frac{\partial x_i(t)/x_i(t)}{\partial \theta_j/\theta_j} = \frac{\partial x_i(t)}{\partial \theta_j} \cdot \frac{\theta_j}{x_i(t)}.$$

For the sensitivity analysis performed in this thesis, the following maximum–norm is used to measure the relative coefficients:

$$\hat{S}^i_j := \|\overline{S}^i_j(t)\|_\infty = \sup_{t\in[0,10h]} \left|\overline{S}^i_j(t)\right|, \tag{2.3}$$

which is also known as Chebyshev norm.

Particularly, the TNF–apoptosis model consists of n=42 states and m=85 reaction parameters. The obtained maximal sensitivity coefficients for a permanent and pulse TNF–input are shown in Figure 2.9.

To identify the most sensitive species x_i, the maximal control coefficients are summed up along all parameters θ_j and normalised with respect to the sensitive species,

$$\breve{S}^i_\Omega = \sum_j \hat{S}^i_j / \max_i(S^i_\Omega), \tag{2.4}$$

see Fig. 2.10(a). Respectively, to identify the most sensitive reaction parameters θ_j, the maximal control coefficients are summed up along all states x_i,

$$\breve{S}^\Omega_j = \sum_i \hat{S}^i_j / \max_j(S^\Omega_j), \tag{2.5}$$

which indicate indicate the overall influence of a reaction parameter on all species, see Fig. 2.10(b).

Results The most sensitive species are all related to the caspase cascade, since here two positive feedback loops amplify small perturbations. In particular, most sensitive are active Caspase 3 (17), FLIP (18) and the complex C2∼FLIP, IAP (34), Procaspase 8 (36), Procaspase 3 (37), active Caspase 8 (38), Bid (39), and the complex C8a∼Bid (40).

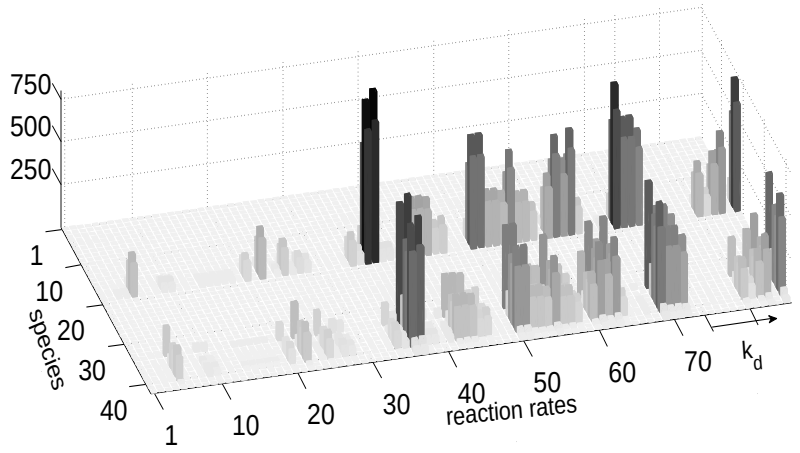

(a) Constant input.

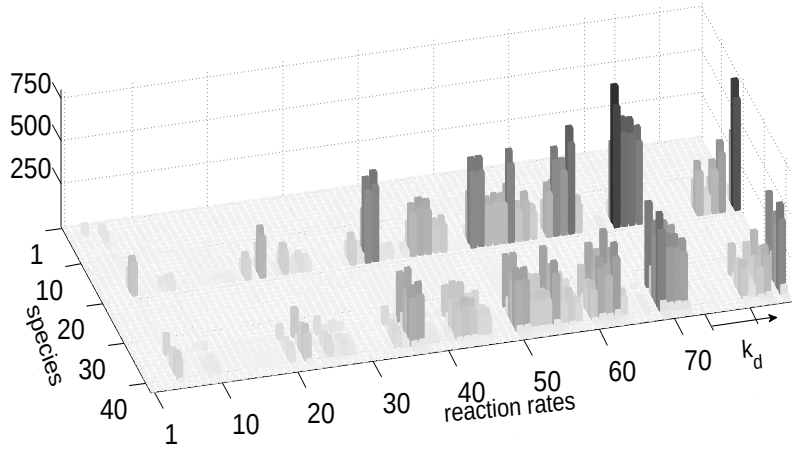

(b) Pulse input.

Figure 2.9: Maximal sensitivity coefficients $\hat{S}^i_j$ of the apoptosis model.

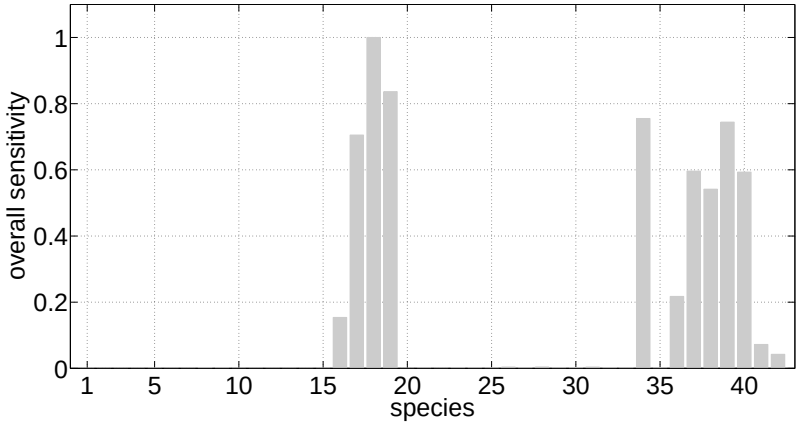

(a) Overall species sensitivities $\breve{S}^i_\Omega$.

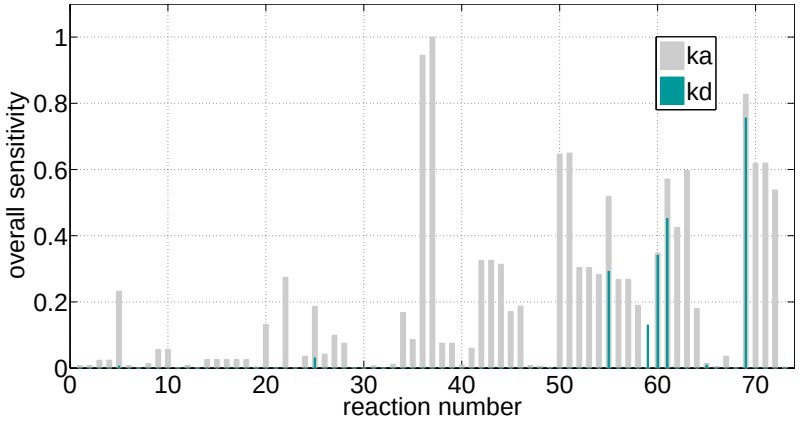

(b) Overall reaction sensitivities $\breve{S}^\Omega_j$.

Figure 2.10: Overall sensitivities.

The most sensitive reactions again are mostly related to the caspase cascade. The NF-κB import (36/37) and IκBα-NF-κBn (50/51) export are very sensitive since they strongly influence the production of caspase inhibitors IAP and FLIP. Further sensitive reactions are the basal expression of IAP (55), Procaspase 8 (60), and Procaspase 3 (61), activation of Procaspase 8 by Complex 2 (62), activation of Procaspase 3 by active Caspase 8 (63), and the interactions of active Caspase 3 with IAP (69), (70), (71), and degradation of active Caspase 8 (72).

2.2.2 Sensitivities of the Apoptosis Characteristics

Of particular importance is the investigation of the influence of the model parameters with respect to the apoptosis characteristics period and dampening of N–C oscillations of NF–κB and the cell death.

The ratio of N–C NF–κB is considered as nonlinear model output and obtained by dividing nuclear and cytoplasm NF–κB concentration, e.g.

$$y_{n/c} := \frac{\text{NF–}\kappa\text{Bn(t)}}{\text{NF–}\kappa\text{B(t)}} = \frac{x_{28}(t)}{x_{25}(t)}.$$

Upon permanent and constant TNF stimulation, e.g. $u(t) = const.$, the oscillations admit a constant period and are dampened, see Figure 2.11.

The period of N–C NF–κB oscillations can be easily determined computing the difference between two neighboured maxima, e.g.

$$\mathrm{y}^{\mathrm{per}}_{\mathrm{n/c}} \sim T\big(\max(2)\big) - T\big(\max(1)\big),$$

whereas averaging the the first N periods yields

$$\mathrm{y}^{\mathrm{per}}_{\mathrm{n/c}} := \frac{1}{N}\sum_N \Big(T\big(\max(N+1)\big) - T\big(\max(N)\big)\Big). \tag{2.6}$$

The dampening of the N–C NF–κB oscillations can be approximated to an exponential decay of the form

$$g(t) = a \cdot \exp(D \cdot t) + b,$$

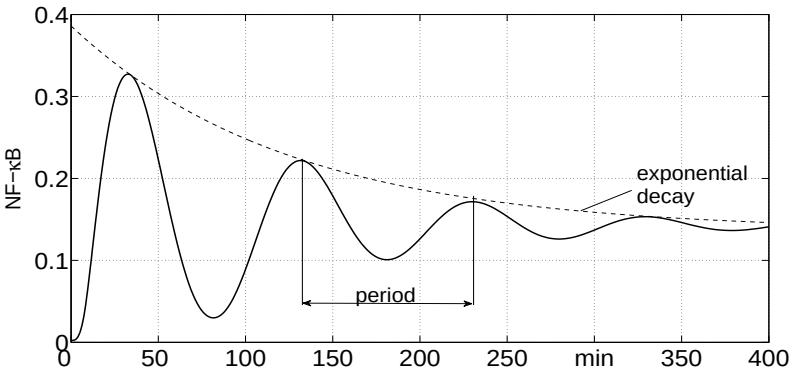

Figure 2.11: Illustration of period and dampening of N–C NF–κB oscillations.

considering the first N maxima using linear regression; D denoted the dampening characteristic

$$\mathrm{y}_{\mathrm{n/c}}^{\mathrm{damp}} := D. \tag{2.7}$$

Cell death is associated to the full activation of effector caspases, subsumed in the apoptosis model to Caspase 3 (x_{17}). The effector caspases cleave other cell compounds and lead finally to the fragmentation of the cell body. Cell death therefore is captured considering a threshold crossing of 0.005μM of active Caspase 3 (x_{17}) and an additional delay of half an hour, such that

$$\mathrm{y}_{\mathrm{cd}} := T(x_{17} \geq 0.005\mu M)) + 0.5h. \tag{2.8}$$

Since the apoptosis characteristics $\mathrm{y}_{\mathrm{n/c}}^{\mathrm{per}}$, $\mathrm{y}_{\mathrm{n/c}}^{\mathrm{damp}}$, and y_{cd} are nonanalytic, their sensitivities with respect to small parameter variations can only determined numerically. Hereby, the finite difference approximation is used, in which the sensitivity coefficient is calculated from the difference of the nominal and perturbed solutions with

$$S_j^y = \frac{\partial y}{\partial \theta_j} = \frac{y(\theta_j + \Delta\theta_j) - y(\theta_j)}{\Delta\theta_j}.$$

Problematically, the numerical values obtained vary significantly with Δ; therefore, a three–point estimation is considered with

$$S_j^y = \frac{\partial y}{\partial \theta_j} = \frac{y(\theta_j + \Delta\theta_j) - y(\theta_j - \Delta\theta_j)}{2\Delta\theta_j},$$

whereas Δ is chosen to 1.5% of the considered parameter. Again, the relative sensitivity coefficients are used and normalised with respect to the maximal sensitivity coefficient:

$$\overline{S}_j^y = \frac{\partial y}{\partial \theta_j} \cdot \frac{\theta_j}{y} / \max_j(\overline{S}_j^y).$$

The obtained sensitivity coefficients for the period $\mathrm{y}_{\mathrm{n/c}}^{\mathrm{per}}$ are presented in Fig. 2.12(a). The most sensitive reaction parameters with respect to N/C NF–κB oscillations are nonactive IKK turnover (25), the NF-κB import (36/37), transcription of IκBα mRNA by nuclear NF-κB (42), translation of IκBα mRNA (43), IκBα import (45/46), and export of nuclear IκB$\alpha\sim$NF–κB (50/51).

The obtained sensitivity coefficients for the dampening characteristic $\mathrm{y}_{\mathrm{n/c}}^{\mathrm{per}}$ are presented in Fig. 2.12(b). The most dampening–sensitive reactions are NF-κB import (36/37), transcription of IκBα mRNA by nuclear NF-κB (42), translation of IκBα mRNA (43), degradation of IκBα mRNA (44), IκBα import (45/46), and export of nuclear IκB$\alpha\sim$NF–κB (50/51).

In Fig. 2.13 are presented the sensitivity coefficients for cell death characteristic y_{cd}. Since cell death along with activation of Caspase 3, the most sensitive reactions due to active Caspase 3 and cell death correspond (see Fig. 2.13). Sensitive reactions are import of NF-κB (36/37), export of nuclear IκB$\alpha\sim$NF–κB (50/51), basal turnover of IAP (55), C8 (60), and C3 (61), and the interactions of active Caspase 3 with IAP (69), (70), (71), and degradation of active Caspase 8 (72).

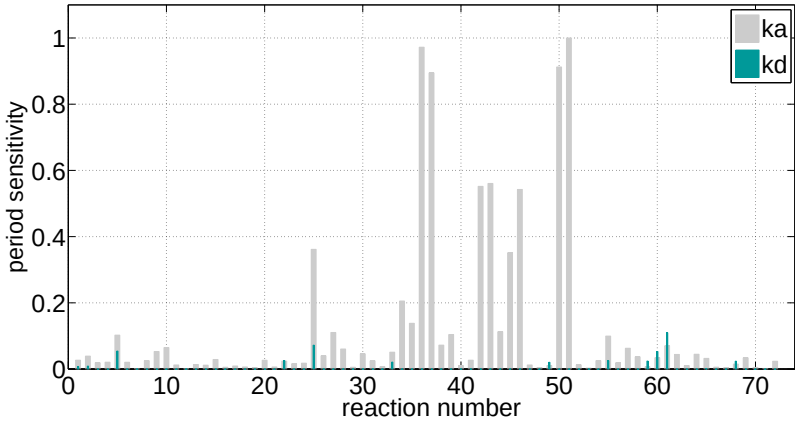

(a) Period sensitivities $\overline{S}_j^{per}$.

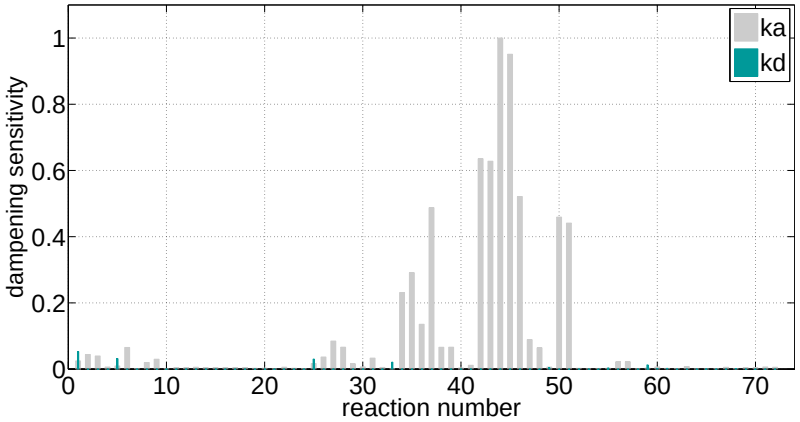

(b) Dampening sensitivities $\overline{S}_j^{damp}$.

Figure 2.12: Period and dampening sensitivities.

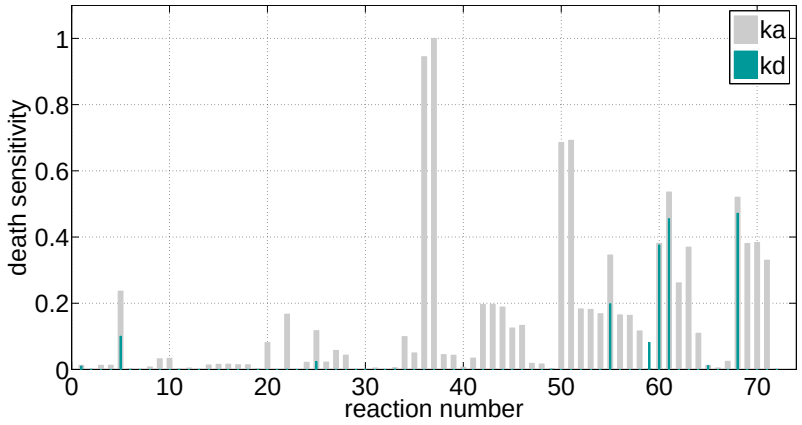

Figure 2.13: Cell death sensitivities $\overline{S}_j^{cd}$.

2.2.3 Gene Expression

Of particular interest is the evaluation of the influence of perturbations of gene expression related parameters, since variations in gene expression capacity from cell to cell are a major source of cell variability. The apoptosis model includes the transcription of 12 species. Some of this expression reactions are directly involved in the regulation of the apoptosis response, and their expression is induced by nuclear NF–κB (A20 mRNA, IκBα mRNA, IAP mRNA, FLIP mRNA). The remainder of the expression reactions are basal.

To identify the influence of gene–expression variations on species concentrations, the sensitivity coefficients for the 12 transcription-related parameters are determined and highlighted in Figure 2.14. Herein, the sensitivity coefficients are normalised to the maximal influence of a parameter $\theta_j \in \mathbb{R}_+^{85}$ on the species x_i

$$\tilde{S}_j^i = \hat{S}_j^i / \max_j(\hat{S}_j^i).$$

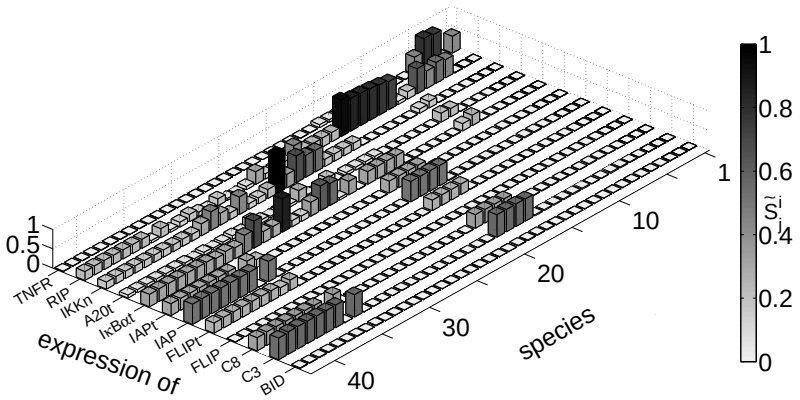

Figure 2.14: Maximal sensitivities of transcription rates. Normalised to maximal species sensitivity.

Results Expression of IAP and Procaspase 3 are very sensitive with respect to caspase cascade related species (16–19 and 34–42). The expression of IκBα mRNA and nonactive IKK are very sensitive with respect to species of the NF–κB module (19–34). Hereby, transcription of IκBα mRNA is most sensitive with respect to level of nuclear NF–κB (28). expression of RIP is very sensitive with respect to species related to TNF–reception and transduction toward Complex 1 and Complex 2 (1–16).

The sensitivity coefficients of the expression rates with respect to period and dampening of NF–κB oscillations and cell death are presented in Table 2.1. Transcription of IκBα mRNA by nuclear NF–κB is the most sensitive expression rate with respect to period and dampening of the NF–κB oscillations, whereas expression of Procaspase 3 is very sensitive with respect to cell death, but does not influence period and dampening. Interestingly, basal transcription of FLIP is less sensitive with respect to the apoptosis characteristics than transcription of FLIP mRNA by nuclear NF–κB, in contrary to IAP.

Expression reaction	**Local Sensitivity** $\overline{S}_j^{per}$	$\overline{S}_j^{damp}$	$\overline{S}_j^{cd}$	S_j^{Ω}
$0 \longrightarrow$TNFR	0.03	0.03	0.01	<0.01
$0 \longrightarrow$RIP	0.10	<0.01	0.24	0.23
$0 \longrightarrow$IKKn	0.36	0.02	0.12	0.19
$0 \overset{\text{NF}-\kappa\text{Bn}}{\longrightarrow}$A20t	0.07	0.07	0.04	0.08
$0 \overset{\text{NF}-\kappa\text{Bn}}{\longrightarrow}I\kappa$B$\alpha$t	**0.55**	**0.64**	0.20	0.33
$0 \overset{\text{NF}-\kappa\text{Bn}}{\longrightarrow}$IAPt	0.01	<0.01	0.18	0.30
$0 \longrightarrow$IAP	0.10	<0.01	0.35	0.52
$0 \overset{\text{NF}-\kappa\text{Bn}}{\longrightarrow}$FLIPt	0.02	0.02	0.17	0.27
$0 \longrightarrow$FLIP	<0.01	<0.01	<0.01	<0.01
$0 \longrightarrow$C8	0.03	<0.01	0.38	0.35
$0 \longrightarrow$C3	0.07	<0.01	**0.54**	**0.57**
$0 \longrightarrow$BID	0.03	<0.01	0.01	<0.01

Table 2.1: All occurring expression reactions and corresponding local sensitivities with respect to the apoptosis characteristics.

To further analyse the sensitivity of IκBα mRNA transcription for larger parameter variations, a univariate sensitivity analysis is performed as shown in Fig. 2.15.

Hereby, period and dampening and the corresponding sensitivities are calculated varying this expression rate from 0.5–fold to 2–fold of the reference value keeping the remainder of reaction rates constant.

The results indicate strong influence over large parameter variations, whereas the sensitivities decline for high expression rates. Therefore, the strong influence of this expression rate holds also for larger parameter variations.

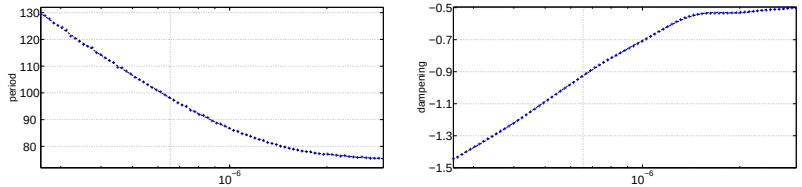

(a) period (c) dampening

(b) period sensitivity (d) dampening sensitivity

Figure 2.15: Univariate sensitivity analysis for IκBα transcription rate (x-axis) with respect to period (left) and dampening (right) of NF-κB oscillations. The reference value is indicated by the dotted vertical line.

2.2.4 Summary Sensitivity Analysis

The local parameter sensitivity analysis performed in this section revealed critical parameters and mechanism of the overall apoptosis model. The most sensitive species and reaction are all related to the caspase cascade, since here positive feedbacks amplify small perturbations. In particular, interactions of active Caspase 3 with IAP and the interactions of FLIP with Complex 2 are very sensitive.

The sensitivity analysis of the apoptosis characteristic cell death (y_{cd}) reveales that the import of NF-κB (36/37), the basal turnover of IAP (55), C8 (60), and C3 (61), and the interactions of active Caspase 3 with IAP (69), (70), (71) are very sensitive.

Furthermore, sensitivity analysis of the N–C NF–κB oscillation characteristics period and dampening uncovers strong influence of NF–κB and IκBα regulating reactions, in particular expression of IκBα mRNA (42,43) by NF–κB, degradation of IκBα mRNA (44), IκBα import (45/46), and export of nuclear IκB$\alpha\sim$NF–κB (50/51).

Comparing the gene expression related reactions among another, transcription of IκBα mRNA by nuclear NF–κB is by far the most sensitive expression rate with respect to period and dampening of the NF–κB oscillations. Not only local, this expression rate is very sensitive with respect to the apoptosis characteristics.

2.3 Bifurcation Analysis

Bifurcation analysis is a powerful method to insight the qualitative behaviour of a dynamical system, in particular to analyse the location and the stability properties of the systems steady states along parameter changes. Thus, the parameter space can be characterised by determining regions that generate qualitatively different steady–state or oscillatory behaviour. The bifurcation analysis plays also an important role measuring robustness properties of dynamical systems.

The bifurcation analysis presented here is applied to the caspase cascade module (Section 2.3.2) and the NF–κB module (Section 2.3.3). In Section 2.3.1, a short introduction to bifurcation analysis is provided. The influence of single–parameter variations is studied on the number, location, and stability of the modules steady states.

2.3.1 Short Introduction

A comprehensive introduction to bifurcation theory can be found in Strogatz [1994].

A continuous dynamical system described as ordinary differential equation system is given by

$$\dot{\underline{x}} = \underline{f}(\underline{x}, \underline{\theta}), \quad f: \mathbb{R}^n \times \mathbb{R}^m \to \mathbb{R}^n$$

with the initial conditions

$$\underline{x}(0) = \underline{x}_o \in \mathbb{R}^n.$$

Hereby, $\underline{f}$ is a smooth vectorfield, $\underline{x} \in \mathbb{R}^n$ denotes the time–dependend states, and $\underline{\theta} \in \mathbb{R}^m$ the system parameters.

To use bifurcation theory to analyse the nonlinear properties of this dynamic system, the steady states (equilibrium points, fixed points) are calculated. These points $\underline{x}^{ss}$ are the points where the vector field vanishes, e.g. the solutions of

$$0 = \underline{f}(.,\theta).$$

An explicit representation of the steady states in terms of an analytical solution is not feasible for large systems. Then, the steady states can only be calculated numerically.

The stability of the steady states along with the local behaviour near the steady states; this is given by the linearisation at the fixed points. Hereby, the Jacobian matrix J of $\underline{f}(\underline{x},\underline{\theta})$, i.e. the partial derivatives of $\underline{f}(\underline{x},\underline{\theta})$ with respect to the states, is calculated at the fixed point.

The eigenvalues of the Jacobian matrix determine the local behaviour. If all eigenvalues have a negative real part, the equilibrium point is asymptotically stable, whereas it is unstable if at least one real part is bigger than zero. In short, a bifurcation occurs when there is a change in the number or the stability of the solutions varying a system parameter.

The simplest type of bifurcations are those involving only one parameter in the system under study called codimension–one bifurcations. The bifurcation parameter will be denoted by λ with $\lambda \in \underline{\theta}$. Then, a local bifurcation occurs at ($\underline{x}^{ss}$, λ^0), if the Jacobian matrix at ($\underline{x}^s s$, λ^0) has an eigenvalue with zero real part. These points are called bifurcation points. If the eigenvalue is equal to zero, the bifurcation is a steady state bifurcation; if the eigenvalue is non–zero but purely imaginary, this is a Hopf bifurcation (Crawford [1991]).

Steady state bifurcations may take several forms, most typical a saddle-node bifurcation, but also transcritical and pitchfork bifurcation (Crawford [1991]).

For high dimensional systems, it is not feasible to study bifurcations analytically; they are studied constructing bifurcation diagrams. The procedure consists of following strategy: first locating an initial fixed point, second calculating a fixed point close to the previous one as the bifurcation parameter λ vary. To follow the equilibrium as the bifurcation parameter varies, numerical continuation algorithms

are used. The steady state then is represented as a function of the bifurcation parameter.

The following analysis is restricted to codimension–one bifurcations; the modules are implemented in Mathematica for analytical analysis, and XPP for the bifurcation analysis with AUTO (continuation).

2.3.2 Bifurcation Analysis of the Caspase–Cascade

A demanded feature of the caspase cascade is bistability, which implies that two stable steady states coexist.

As explained in Section 1.4.2, the caspase cascade has been changed. In particular, CARP interactions have been removed (see Section 1.4.1), and Bid cleavage is taken into account, and the caspase reaction parameters have been changed (see Table 5.3).

To proove bistability of the changed caspase cascade, a bifurcation analysis is performed. Herefore, only the reactions downstream of late complex C2 are considered (reactions 55 and 60–73, see Table 5.4). The model input is set constant to zero.

Results The modified caspase cascade is bistable at the new parameter set. Thus, the caspase cascade possesses two stable steady states, see Fig. 2.16 and 2.17, of which one corresponds to the resting steady state (no active caspases) the other to the "dead" steady state (active caspase).

The bistability property of the caspase cascade however may change for large variations of critical parameters, e.g. the positive feedback parameters ka63 and ka64. Raising the parameter ka63 or ka64, e.g. accelerating the reactions

$$C8a + C3 \xrightarrow{ka_{63}} C8a + C3a,$$

or

$$C3a + C8 \xrightarrow{ka_{64}} C3a + C8a,$$

respectively, causes a transcritical bifurcation. Hereby, the resting steady state turns unstable, see Fig. 2.16. Lowering the reaction parameters ka63 or ka64, a saddle node bifurcation occurs, such that

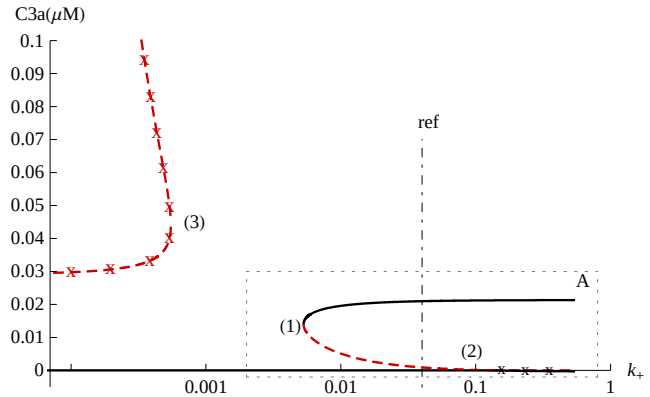

(a) Bifurcation diagram of reaction parameter ka64.

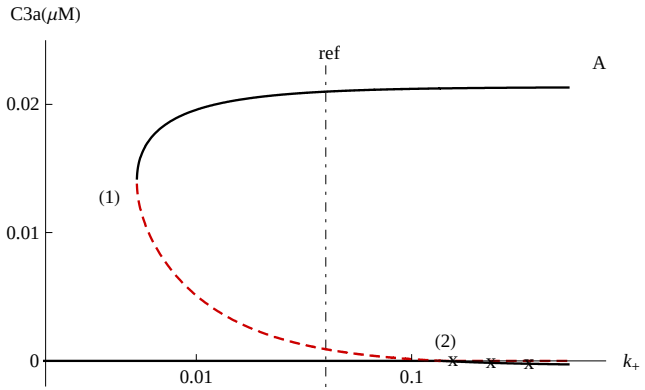

(b) Magnification of inset A.

Figure 2.16: Bifurcation diagram of the caspase cascade. k_+ denotes positive feedback parameter explained in the text. Dashed red branches indicate instability, black branches stability. Branches marked with 'x' are not positive, e.g. at least one species concentration is negative and thus not relevant. The reference parameter is indicated by the dot–dashed, vertical line. (1) and (3): Saddle node bifurcation, (2) transcritical bifurcation.

for lower rates no other stable steady state exists than the resting steady state, e.g. caspase casscade cannot be triggered.

Another critical parameter is the basal expression rate of IAP, see Fig. 2.17.

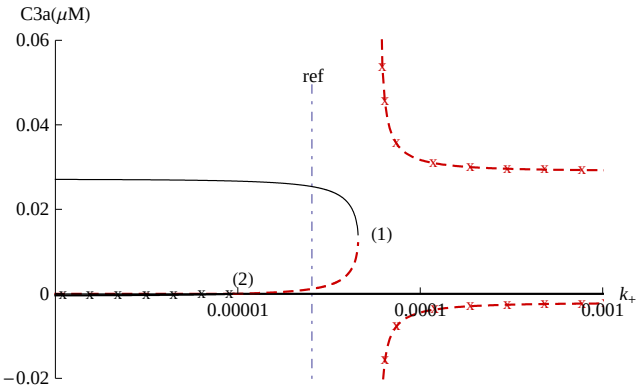

Figure 2.17: Bifurcation diagram of the caspase cascade. k_+ denotes IAP expression rate as explained in the text. Dashed red branches indicate instability, black branches stability. Branches marked with 'x' are not positive, e.g. at least one species concentration is negative and thus not relevant. The reference parameter is indicated by the dot–dashed, vertical line. (1): Saddle node bifurcation, (2) transcritical bifurcation.

For high IAP expression rates, a large amount of Caspase 3 inhibitors is provided, such that caspase cascade cannot be triggered. Low expression rates of IAP cause instability of the resting steady state, e.g. caspase cascade is activated from the first.

2.3.3 Bifurcation Analysis of the NF–κB Module

Of particular interest is the investigation of N–C NF–κB oscillations (N–C oscillations). At the local parameter set, these oscillations are damped. The sensitivity analysis in Section 2.2 showed that some parameters strongly influence dampening of this oscillations, in particular transcription of IκBα mRNA, translation, degradation and

import of IκBα, and export of nuclear IκB$\alpha\sim$NF-κB.

Therefore, the NF–κB module is investigated with a codimension–one bifurcation analysis. Herefore, only reactions downstream early complex C1 are considered (reactions 8–9, 25–51, see Table 5.4). The input is the concentration of early Complex 1 (C1).

Preparation The NF–κB module is implemented in XPP. The states are scaled such that the concentrations are about 1 μM. The input (concentration of C1) is set constant with 0.001μM (in the scaled model C1=1μM) equivalent to a high TNF–input (about 100 ng/ml).

Furthermore, an implicit conservation law is concealed in the system resulting in a zero eigenvalue of the Jacobian; this is tackled assuming a turnover for the complex IκB$\alpha\sim$NF–κB, e.g.

$$0 \underset{kd}{\overset{ka}{\rightleftharpoons}} \text{I}\kappa\text{B}\alpha\sim\text{NF}\text{–}\kappa\text{B}$$

with ka=1.74e-05 [μM/s], kd=1e-4 [1/s] such that the corresponding initial concentration is kept.

Results The system goes through Hopf–bifurcations for high transcription rates (Fig. 2.18) and high translation rates (Fig. 2.19) of IκBα, and low degradation rates of IκBα (Fig. 2.20). In the region bounded by the two supercritical Hopf–bifurcations, stable limit cycles occur.

For a range of 2.5–fold and 160–fold of the (reference) transcription rate of IκBα mRNA, e.g.

$$\text{NF}\text{–}\kappa\text{Bn} \longrightarrow \text{NF}\text{–}\kappa\text{Bn}+\text{I}\kappa\text{B}\alpha\text{t},$$

and translation rate of IκBα, e.g.

$$\text{I}\kappa\text{B}\alpha\text{t} \longrightarrow \text{I}\kappa\text{B}\alpha\text{t}+\text{I}\kappa\text{B}\alpha,$$

the NF–κB oscillations are stable and undamped, see Fig. 2.18(a) and 2.19(a). The period of the stable limit cycles (Fig. 2.18(b) and 2.19(b)) varies from about 75 min to 40 min.

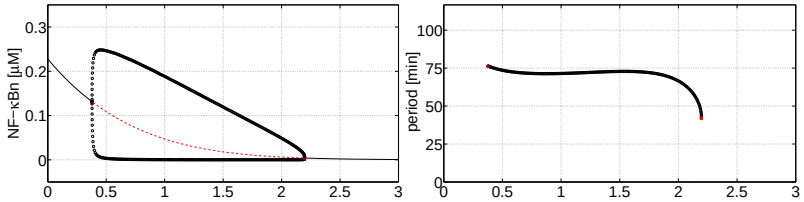

Figure 2.18: Transcription of IκBα mRNA.

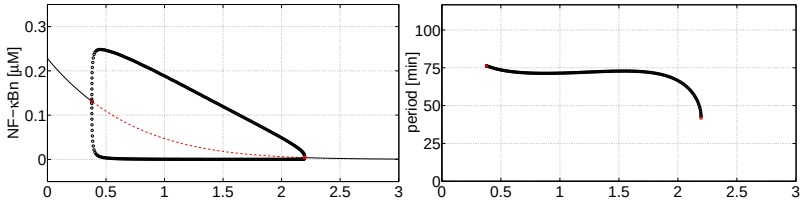

Figure 2.19: Translation of IκBα mRNA.

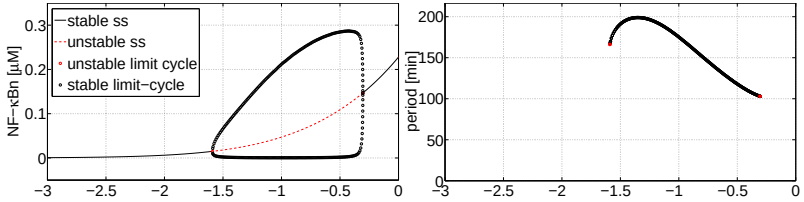

Figure 2.20: Degradation of IκBα mRNA.

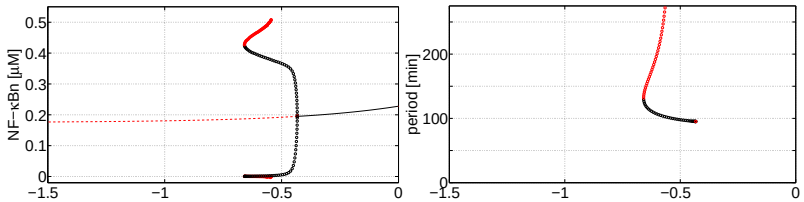

Figure 2.21: Degradation of IκBα.

Figure 2.22: Bifurcation diagrams of the NF–κB module. X-axis: 10^x–fold reaction rate with respect to the reference value. Left: steady state concentrations of nuclear NF–κB as function of the bifurcation parameter. Right: corresponding period of NF–κB oscillations.

For a range of 1/2.5–fold and 1/50–fold of the (reference) degradation rate of IκBα mRNA, e.g.

$$\text{I}\kappa\text{B}\alpha\text{t} \longrightarrow 0,$$

the NF–κB oscillations are stable and undamped. The period varies from about 105 min to 170 min.

The system also admits a Hopf–bifurcation for low degradation rates of IκBα (Fig. 2.21). For degradation rates of IκBα lower than 1/2.5–fold, the system admits stable limit cycles, though lowering the degradation rate can cause unstable limit cycles. For the remainder of the modules parameter, no bifurcations occur in the upper and lower decade with respect to the reference parameter values.

Thus, the qualitative shape of the NF–κB response can change for large variations of IκBα–related parameters. The obtained results have been compared and qualitatively validated with respect to the overall TNF–induced apoptosis model in simulation studies. The qualitative shape of the bifurcation diagrams also hold for the complete model, whereas the limit cycle amplitudes and the range within limit cycles occur deviate from the studies of the modified subsystem. One reason of this deviations relies in the feedback of the proapoptotic response, e.g. the formation of early complex C1 is strongly diminished by active Caspase 3. A bifurcation analysis of the complete model should be addressed in further studies.

2.4 Summary & Conclusions

TNF–induced apoptosis signalling is double–edged. TNF–stimulation leads to the formation of the early Complex 1, which forms the pedestal for the two concurring apoptosis pathways. The early Complex 1 induces the activation of NF–κB, whereas late Complex 2 triggers activation of caspases. The anti–apoptotic response consists of activation and translocation of NF–κB in the nucleus. Here, NF–κB induces the transcription of apoptosis inhibitors IAP and FLIP.

The analysis performed in this chapter outlined the particular role of IκBα with respect to the regulation of nuclear factor κB. The interactions of IκBα with NF–κB establish a negative feeback that drives oscillations of the nuclear factor κB. The expression of IκBα, e.g.

translation and transcription of IκBα mRNA, are not only very sensitive with respect to dampening and period of NF–κB oscillations, but also govern the qualitative shape of these oscillations. High expression levels increase the duration of the oscillations, and for even higher expression levels stable and undamped oscillations occur.

At the local parameter set, the oscillations are damped with a period of about 100 min in accordance with the single cell experiments of Nelson et al. [2004] and Sillitoe et al. [2007]. The local parameter sensitivity analysis showed that expression of IκBα mRNA (42,43) by NF–κB, degradation of IκBα mRNA (44), IκBα import (45/46), and export of nuclear IκB$\alpha\sim$NF–κB (50/51) are the most sensitive reactions.

The pro–apoptotic response is triggered by late Complex 2; delayed by about one hour, late Complex 2 activates Procaspase 8, in turn activating effector Caspase 3. Activated Caspase 3 acts in terms of a positive feedback loop onto Procaspase 8 resulting in an all–or none mechanism, whereas the cells' caspase pool is activated rapidly within 30 min. The bifurcation analysis validated that the changed caspase cascade is bistable. The most sensitive reactions with respect to caspase activation and therefore cell death are the import of NF-κB (36/37), the basal turnover of IAP (55), C8 (60), and C3 (61), and the interactions of active Caspase 3 with IAP (69), (70), (71).

Chapter 3

Cell Variability and Population Heterogeneity

In systems biology, mathematical models based on ordinary differential equations are used frequently to describe metabolic or signal transduction processes. These biochemically structured continuum models contain a significant amount of biological details of the regarded process and describe the dynamics of the intracellular concentrations of an average cell. Whereas their exist numerous well–developed computational and theoretical tools for the purpose of simulation and analysis of such ODE systems, their quantitative predictability is limited. Owing to fluctuations in network components from cell–to–cell and over time within a single cell, even isogenic cells supposed to the same environmental conditions exhibit variability.

For a number of biological processes, cell variability can be very large (Dower and Qwarnstrom [2003]), and thus average cell behaviour as described by continuum models may be a poor indicator of the way individual cells respond. In addition, the majority of available experimental techniques collect measurements from cell populations; population dynamic and population properties however are biased by the effect of cell variability. For a predictive understanding of cellular processes, it is therefore important that cell variability is accounted in both experiment and modeling.

In this chapter, a cell–ensemble model for a Kym–1 cell population

is derived accounting for population heterogeneity in TNF–induced apoptosis signalling. In Section 3.1 a discourse of cell variability and population heterogeneity is provided. In Section 3.2, the sources of cell variability and population heterogeneity are discussed. In Section 3.3, different approaches aiming to model cell variability are reviewed. In Section 3.4, the sources of population heterogeneity specific to TNF–induced apoptosis are discussed. In Section 3.5, a predictive statistical model is derived accounting for Kym–1 cell population heterogeneity.

3.1 Introduction

Variability describes the phenomena that cells of the same type exhibit individuality and differences in behaviour when supposed to similar conditions. As early as 1945, Delbrück observed variations in the number of produced phages in infected E. coli from cell to cell. Hereafter, variability has been shown for a wide variety of cellular processes in different cell types ranging from bacterial cells (Swain et al. [2002]) to complex mammalian cells (Ramsey et al. [2006]).

For a number of biological processes, cell variability can be large and decisive; when for example cell response depends on a positive feedback, e.g. Tat transactivation in HIV live cycle (Weinberger et al. [2005]) or caspase activation in TNF–induced apoptosis, small fluctuations of otherwise identical cells can be amplified resulting in bifurcating phenotypes, e.g. latent or productive HIV–1 infection (Weinberger et al. [2005]) or respectively alive or dead cell.

Many biochemical techniques such as Western Blotting and Electrophoretic Mobility Shift Assays (EMSA) measure average responses combining many cells for analysis, all of which contribute in a different way to the overall observed behaviour. Single cell all or none decisions however or oscillatory behaviour can be masked in the average response. Population dynamic and population properties are biased by the effect of cell variability.

An example of the difference of single cell behaviour and population response is given in Fig. 3.1. Stimulation of cells with Tumor Necrosis Factor α (TNF–α) induces activation of the transcription factor NF–κB. Characteristically, the transcription factor translocates between the nucleus and cytoplasm, whereas its localisation can be monitored at single cell level using time-lapse fluorescence microscopy (coloured lines).

Single cells exhibit variability in period and amplitudes of these oscillations; averaging the individual cell responses of only 24 cells results in a population dynamic where individual NF–κB oscillations are masked (black line). Such a population–average dynamic is obtained with EMSA allowing to monitor the levels of nuclear NF–κB. For the purpose of a predictive understanding of cellular processes on the one and evaluation of population data on the other hand it is necessary to investigate and to mathematically describe cell variability. For this, it is important to first understand the sources of cell variability.

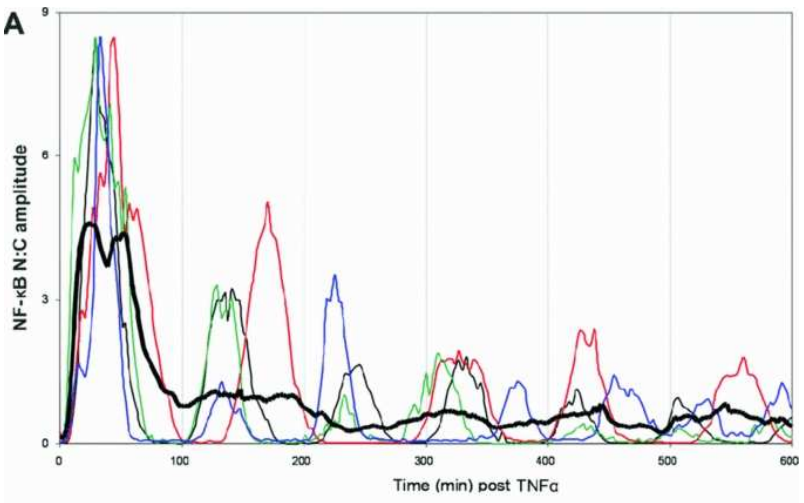

Figure 3.1: Wash–out effect. Single–cell level investigation of NF–κB nucleus/cytoplasmic oscillations (Sillitoe et al. [2007]). Continuous stimulation of SK–N–AS–cells with 10 ng/ml TNF–α.

3.2 Sources of Cell Variability

Genetic differences are one of the main factors responsible for cellular heterogeneity, since a different set and number of genes lead to different cellular composition and thus different behaviour. Genetic differences are of particular importance in single cell organisms such as bacteria.

Another important factor for cell heterogeneity is the environment. Cells exposed to different environmental conditions, such as temperature, pH, and nutrient concentrations, admit different phenotypes. Non-uniform extracellular environmental conditions constitute therefore a source of cell variability which is of particular importance in large scale bioreactors.

We will not further consider genetic or environmental heterogeneity, since the focus of our interest are isogenic mammalian cell populations such as Kym–1 cells in a fixed environment.

However, even cells or organisms with the same genes, in the same environment, with the same history, display variations in form and behaviour. Due to for example unequal partitioning of the mother cell, cells of an isogenic cell population contain different amounts of RNA, proteins, metabolites, and mitochondria. Therefore, cellular phenotype vary from cell–to–cell and thus cellular behaviour. This type of variability caused by preexisting cell–to–cell variations is termed *extrinsic* heterogeneity.

Finally, cells which have the same state may also exhibit variability. Many cellular components, especially regulatory molecules, exist at very low concentrations and hence, the involved reactions are inherently noisy or stochastic. This type of heterogeneity is called *intrinsic* heterogeneity.

A cellular response such as the TNF–induced apoptosis is based on the underlying signal transduction network. Such networks in general involve gene expression processes, either in form of direct regulation or due to production of network components. A major contribution to cellular variability originates from this process from DNA to RNA to protein.

Levsky et al. [2002] profiled gene expression levels in single cells and provided evidence of variable expression patterns in isogenic cells. Their dual–reporter measurement technique allowed to investigate

the sources of variable gene expression. Variations originates from extrinsic and intrinsic sources.

Extrinsic noise in gene expression arises from fluctuations in regulatory proteins and polymerases, and has a global effect, e.g. influence all expression processes occurring in the cell (Elowitz et al. [2002]). Intrinsic noise arises from the stochastic nature of the biochemical process of gene expression and causes identical copies of a gene to express at different levels (Elowitz et al. [2002]). Variable gene expression cause that the amount of proteins vary from cell to cell and over time within single cell. Gene expression variability is of particular importance, since also the TNF response is directly regulated at gene expression level (NF–κB) and its components are continuously produced.

Rosenfeld et al. [2005] studied gene expression in E. coli cells over long time and provided insights into the relative amplitude and time scales of intrinsic and extrinsic noise. This study showed that extrinsic and intrinsic noise act over different time scales. Rapid fluctuations (autocorrelation 10 min) in the number of mRNA result from intrinsic stochastic. The time scale for extrinsic noise factors (autocorrelation 40 min) is in the range of the cell cycle length for E. coli, which suggests that whatever factors result in global noise persists on average for about one cell cycle (Raser and O'Shea [2005]). This study suggests that extrinsic noise may affect cellular phenotypes more strongly than intrinsic noise, at least in E. coli (Rosenfeld et al. [2005]).

Colman-Lerner et al. [2005] analysed the relative contribution of global noise and pathway-specific noise to cell-to-cell variation in a cell-fate decision, in particular the pheromone response pathway in yeast. They showed that preexisting differences in the cell–cycle position and gene expression capacity of individual cells at the time of pathway induction dominate cell–cell variations rather than pathway specific or gene expression intrinsic noise. Cell–cell variability herein is therefore dominated by initial differences between cells.

3.3 Modeling Cell Variability

The traditional approach of single cell modeling is based on ordinary differential equations (ODE) describing the dynamics of the intracellular concentrations and their coupling with external stimuli such as concentration of a signal or nutrients in an average cell. The question of how single cell variability and population dynamic can be accurately described depends on the regarded cellular network and involves a choice or decomposition of the relevant source of variability.

Inherent stochastic due to small molecule numbers can be quantitatively captured considering Gillespie algorithms. Stochastic kinetic models have been applied for wide range of cellular networks, including a simplified version of the NF–κB model by Hayot and Jayaprakash [2005]. Such a stochastic approach allows to study the impact of inherent stochastic in networks; however, it does not account for population heterogeneity emerging from preexisting cell–to–cell variations.

With a different class of models, cell population balance (CPB) models, it is possible to include an isolated, extrinsic effect causing cell population heterogeneity (such as cell division process, the unequal partitioning of mother cell content at cell division, see Mantzaris [2007]) in a deterministic single cell model. The resulting CPB models consist of first-order, hyperbolic, partial integro-differential equations describing the time evolution of the cell property distribution, which are typically nonlinearly coupled with integro-ordinary differential equations describing the dynamics of the extracellular environment (Mantzaris [2005]). Such formulations are characterised by significant mathematical complexity and their numerical simulation represents a challenging task (Mantzaris [2005]). Therefore, CPB models have been applied only for lowdimensional cellular processes.

A statistical description of cell–to–cell gene expression variability is suggested by Mar et al. [2006]. Herein, the variation in the number of mRNA transcripts in each cell at a single time point is described as Poisson random variable. With other words, the probability that a cell contains a number N of mRNA transcripts at a single time point is given by the Poisson distribution. This distribution is skewed to the right, and is closely related to Gaussian normal distribution.

For our purpose to describe cell heterogeneity for the TNF–induced apoptosis in a population of Kym–1 cells, we will follow a statistical approach based on preexisting cell–to–cell variations Henson et al. [2002].

3.4 Cell Variability in TNF–induced Apoptosis

The TNF–induced apoptosis model is a single cell model based on ordinary differential equations. It describes the TNF–induced cell response in an average Kym–1 cell, e.g. the induction of both a pro–apoptotic pathway leading to activation of caspases and a anti–apoptotic pathway activating the transcription factor NF–κB.

Cells exposed to TNF display variability in NF-κB oscillation amplitudes and period, as shown in Sillitoe et al. [2007], and diplay cell death distributions characteristic to the TNF–input (compare Fig. 1.5).

In order to reproduce the population heterogeneity of Kym–1 cells in TNF response, the central question is whence cell variability originates from in TNF–signalling. Not considering environmental sources, variability here in general may arise from inherent stochastic of the biochemical TNF–induced apoptosis network or from preexisting cell–to–cell variations.

The influence of inherent stochastic has been observed already for a simplified version of the NF–κB module Hayot and Jayaprakash [2005]. The authors demonstrated that intrinsic fluctuations are small in the model with strong transcription, as proposed by Hoffmann et al. [2002] which template the overall TNF–induced apoptosis model. With other words, since the amplitudes of intrinsic fluctuations are small, the rapid fluctuations due to random reaction events are averaged out over time; thus, inherent stochastic does not suffice to explain cell variations in NF–κB oscillation amplitude and period.

In contrary to intrinsic noise, the effect of extrinsic fluctuations can be significant: Hayot and Jayaprakash [2005] showed that cell–to–cell fluctuations of the initial amount of cellular NF-κB and the amount of activated IKK affect both amplitudes and period of NF–κB oscillations. Moreover, the local parameter sensitivity analysis in Chapter 2 outlined the influence of small fluctuations in expression

rates and therefore initial concentrations on the apoptosis characteristics period and dampening.

Therefore, a natural assumption is that cell population heterogeneity in TNF–induced apoptosis is driven by cell–to–cell variations, which in fact have been shown to exist, see Fig. 3.2. These variations presumably originate from variations in gene expression rather than from degradation, since cell–cell variations in gene expression come along with cell–to–cell variations in phenotype. Hereby, extrinsic variations dominate total gene expression noise rather than fast intrinsic fluctuations. This extrinsic fluctuations are manifested in variations of regulatory molecules such as abundance of transcription factors or RNA polymerases, lasting for about one cell cycle length.

This leads the way for statistical approach to capture Kym–1 cell population heterogeneity: preexisting cell–to–cell variations in gene expression drive variability whereas gene expression within a single cell is constant over the time scale from apoptosis induction to apoptosis execution (about 15 hours respectively 1/4 cell cycle length of Kym–1 cells).

To this end, the cell–to–cell variations of Kym–1 cells need to be characterised in terms of a probability distribution.

3.4.1 Assigning a Distribution for Cell–Cell Variations

The number of TNF–receptors has been measured experimentally in a population of Kym–1 cells, see Fig. 3.2. Interestingly, Kolmogorov-Smirnov normality test confirmed with a 95% significance the hypothesis of the TNFR–receptor number being lognormally distributed (p–value=0.34$\gg$0.05) in a Kym–1 cell population (for details, see Appendix). In contrary to the symmetric Gaussian normal distribution $N(\mu,\sigma)$, the lognormal distribution $\Lambda(\mu,\sigma)$ is skewed to the right. Skewed distributions are particularly common when mean values are low, variances large, and values cannot be negative (Limpert et al. [2001]), as in the case of molecules and their concentrations.

The lognormal distribution is defined as the distribution of a random variable whose logarithm is normally distributed. For random

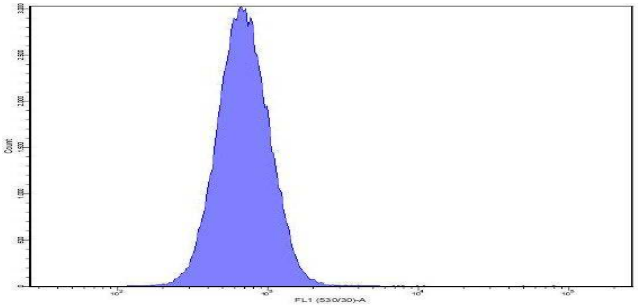

Figure 3.2: Snapshot of TNF–receptor number in a Kym–1 cell population. Counted are number of cell displaying a marker intensity, which is considered to be proportional to receptor number. Schliemann [2007], IZI Stuttgart, unpublished data.

variables X and Y with X>0 and $Y = \ln(X)$ holds:

$$Y \text{ is } N(\mu,\sigma)\text{–distributed} \Leftrightarrow X \text{ is } \Lambda(\mu,\sigma)\text{–distributed.}$$

The density function of the continuous lognormal distribution is given by:

$$f_{\mu,\sigma}(x) = \begin{cases} \dfrac{\exp(-(\ln\ x-\mu)^2/(2\sigma^2))}{x\sigma\sqrt{2\pi}} & (x>0) \\ 0 & (x\le 0) \end{cases}$$

with the following characteristics:

	Normal D.	**Lognormal D.**
Mean	μ	$e^{\mu+\frac{\sigma^2}{2}}$
Variance	σ^2	$e^{2\mu+\sigma^2}(e^{\sigma^2}-1)$
Median	μ	e^{μ}

For further details to lognormality tests and confidence intervals, see Appendix. Figure 3.2 diplays the measured marker intensity considered to be proportional to the receptor number. The probe is lognormal distributed with mean $\mu_I = \ln(819)$ and standard deviation $\sigma_I = 0.31$.

The relation of receptor number and the corresponding expression rate is obtained considering the turnover of the TNF–receptor (TNFR), e.g.

$$0 \underset{d_T}{\overset{p_T}{\rightleftharpoons}} \text{TNFR}$$

where the constant p_T denotes the expression rate, and d_T the degradation rate. For the steady–state receptor concentration TNFR_{ss} holds

$$\text{TNFR}_{\text{ss}} = \frac{\text{p}_\text{T}}{\text{d}_\text{T}}, \tag{3.1}$$

and therefore the receptor number TNFR_{ss} is linear proportional to its expression rate p_T.

The distribution parameters for expression rate (μ_{p_T} and σ_{p_T}) are obtained considering that the spread of the intensity and spread of expression rate correspond (variable degradation is not considered). Hereby, the variation-coefficient VarK(X) indicates the normalised spread, e.g.

$$\text{VarK}(X) := \frac{\sqrt{\text{Var(X)}}}{\text{E[X]}} = \exp(\sigma^2 - 1). \tag{3.2}$$

Note that VarK(X) is simply a function of σ. Therefore we obtain for the spread of p_T:

$$\begin{aligned} &\text{VarK}_\text{I} \overset{!}{=} \text{VarK}_{\text{p}_\text{T}}, \\ &\Leftrightarrow \sqrt{\exp(\sigma_I^2 - 1)} \overset{!}{=} \sqrt{\exp(\sigma_{p_T}^2 - 1)}, \\ &\Leftrightarrow \sigma_I = \sigma_{p_T} \\ &\sigma_{p_T} = 0.31. \end{aligned} \tag{3.3}$$

For the mean μ_{p_T} we obtain:

$$\begin{aligned} &E[X] := \exp\left(\mu + \frac{\sigma^2}{2}\right), \mu = \ln(\text{E[X]}) - \frac{\sigma^2}{2}. \\ &E_{p_T}[X] = 2.3 * 10^{-11}, \sigma_{p_T} = 0.31, \\ &\mu_{p_T} = \ln(2.19 \cdot 10^{-11}). \end{aligned} \tag{3.4}$$

The resulting expression rate distribution of TNF–receptors is displayed in Figure 3.3.

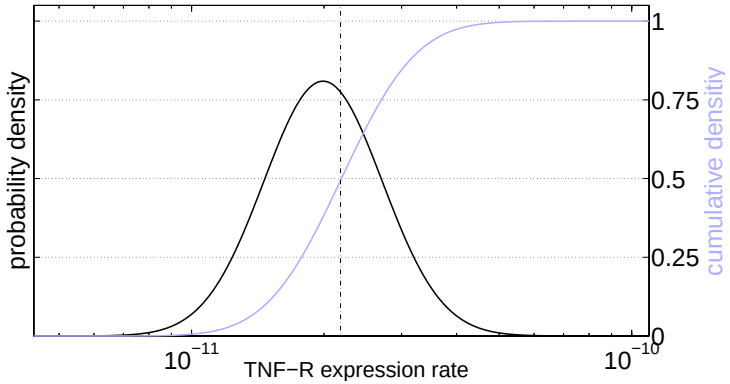

Figure 3.3: Resulting distribution the receptor–expression rate in a Kym–1 population. Probability density (black) and cumulative density (grey) distributions.

In summary, cell–to–cell variations in the TNF–receptor number arise from cell–to–cell variations in receptor expression capacity. The TNF–receptor number is lognormally distributed within a Kym–1 population, and since expression rate and receptor number are linearly proportional, expression rate is also lognormal distributed within a Kym–1 population. Expression capacity vary from cell to cell but not within a single cell. Since the cell–cell variation of TNF–receptor number has been determined experimentally, we will include this information in the following statistical population model.

3.5 Population Model

The TNF–induced apoptosis machinery in a single cell is captured by the ordinary differential equation (ODE) system described as biochemical reaction network as

$$\dot{\underline{x}}(t) = \underline{f}(\underline{x}(t), \underline{\theta}) + u(t), \;\; \underline{x} \in \mathbb{R}^n_+, \; u(t) \in \mathcal{L}_2\left[0, \infty\right], \; t \geq 0$$

with the initial condition

$$\underline{x}(0) = \underline{x}_o, \; \underline{x}_o \in \mathbb{R}^n_+,$$

and the system outputs

$$\underline{y}(t) = \underline{x}(t) \text{ (states)},$$
$$y_{n/c}(t) = \frac{x_{28}(t)}{x_{25}(t)},$$

and nonanalytic system characteristics

$$\mathrm{y}^{\mathrm{per}}_{\mathrm{n/c}}, \; \mathrm{y}^{\mathrm{damp}}_{\mathrm{n/c}}, \; \mathrm{y}_{\mathrm{cd}}.$$

Hereby, $\underline{x}(t)$ represents the n species concentrations and $u(t)$ refers to the (non–negative) external concentration of TNF–α; $\underline{\theta} \in \mathbb{R}^m_+$ denotes the reaction parameters such as expression, degradation, and association rates.

Keeping the networks topology fixed (e.g. $\underline{f}$), single cell dynamic and behaviour only depends on the reaction parameters $\underline{\theta}$, the initial values $\underline{x}_o$ and the (non–negative) TNF–input $u(t)$, and will be denoted with χ^i:

$$\chi^i = \chi\big(\underline{\theta}^i, \underline{x}^i_o, u^i(t)\big) := \left\{ \begin{array}{l} \dot{\underline{x}}^i(t) = f\big(\underline{x}^i(t), \underline{\theta}^i\big) + u^i(t) \\ \underline{x}^i(0) = \underline{x}^i_0 \\ \underline{y}^i \end{array} \right. ,$$

whereas $\underline{y}$ represents the system outputs and characteristics.

The cell population is modelsed as N individual cells (indexed by i) of the same type,

$$\mathrm{Pop} = \{\chi^1, \chi^2, ..., \chi^N \mid N \in \mathbb{N}, \chi^i = \chi\big(\underline{\theta}^i, \underline{x}^i_0, u^i(t)\big)\}. \tag{3.5}$$

Considering an homogeneous environment (TNF–input) for all cells of the population, e.g.

$$u^i(t) = u(t) \; \forall i = 1(1)N, \tag{3.6}$$

thus the single cell behaviour only depends on the (individual) reaction parameters and the initial conditions, e.g.

$$\chi^i = \chi\big(\underline{\theta}^i, \underline{x}^i_0, u(t)\big). \tag{3.7}$$

The single cells of a population are identical exept for some specific reaction rates $\underline{p}$ with $\underline{p} \subseteq \underline{\theta}$ being distributed within a cell population. Therefore, cell individuality originates only from on a subset of the reaction parameters differing from cell to cell (those are indexed with i). Also, the individual parameter set $\underline{p}^i$ in general implies individual initial conditions $\underline{x}^i_o$ (which may not be trivial to calculate). Hence, the generalised statistical population model in a homogeneous environment is given by:

$$\mathrm{Pop} = \{\chi^1, \chi^2, ..., \chi^N \mid N \in \mathbb{N}, \chi^i = \chi\big(\underline{p}^i, \underline{x}^i_o, u(t)\big)\}. \tag{3.8}$$

whereas $\underline{p}^i$ are assigned to the distributions $\underline{D}$

$$\underline{p}^i \;\sim\; \underline{D} \; \forall i = 1(1)N, \tag{3.9}$$

e.g. uniform, normal, or lognormal distributions.

The population dynamics $\underline{y}_{Pop}(t)$ can be easily computed averaging the individual dynamics, e.g.

$$\underline{y}_{Pop}(t) = \frac{1}{N} \sum_i \underline{x}^i(t). \tag{3.10}$$

From the individual characteristics $\mathrm{y}^{\mathrm{i}}_{\mathrm{per}}$, $\mathrm{y}^{\mathrm{i}}_{\mathrm{damp}}$, and $\mathrm{y}^{\mathrm{i}}_{\mathrm{cd}}$, the distributions for the cell population are derived in form of probability densities or cumulative densities.

3.5.1 Kym–1 Cell Population Model

Based on the general statistical population model, a population model specific to Kym–1 cells is derived here. Kym–1 cells (χ^i) differ in their TNF–receptor expression capacity (p_T^i) and therefore in the initial receptor number x_{To}^i according to the experimental measurements (Section 3.4.1). The receptor expression capacities are assigned to the lognormal distribution $\Lambda_T\big(\mu_{p_T}, \sigma_{p_T}\big)$, e.g.

$$p_T^i \sim \Lambda_T\big(\mu_{p_T}, \sigma_{p_T}\big) \ \forall\, i = 1(1)N, \tag{3.11}$$

with

	mean μ	**st. deviation σ**	**median**
$\Lambda_T(\mu_{p_T}, \sigma_{p_T})$	ln(2.19e-11)	0.31	2.3e-11

The initial receptor number x_{To}^i of cell χ^i follows from Equation (3.1), e.g.

$$x_{To}^i = \frac{p_T^i}{d_T}. \tag{3.12}$$

This basic statistical description of a Kym–1 cell population takes into account only cell–cell variations of the receptor expression capacity. The population effect of variable receptor expression however is too small to reproduce the observed population phenomenas, since this expression rate is not very sensitive with respect to period ($y_{n/c}^{per}$) and dampening ($y_{n/c}^{damp}$) of NF–κB oscillations and cell death (y_{cd}), see Table 2.1, Section 2.2.3.

Unfortunately, no data is available for distributions of other components or expression rates of the TNF–induced signalling network than the TNF–receptor. Neither from a biological nor a modeling perspective it is meaningful to assume that all components and expression rates to vary from cell to cell. Negative feedbacks and post-translational regulation mechanisms has been demonstrated to reduce cell-to-cell fluctuations thus increasing the stability of the network (Becskei and Serrano [2000]); with other words, components not necessarily fluctuate.

Table 2.1 shows all expression reactions and the corresponding sensitivity coefficients with respect to the apoptosis characteristics. Hereby, expression of IκBα mRNA by NF–κB is the most sensitive reaction with respect to dampening and period of NF–κB oscillations, and very sensitive with respect to time point of cell death.

Therefore, cell–to–cell variability of IκBα–gene expression is considered as second extrinsic variable for the statistical model. Since this gene expression is directly regulated via NF–κB, cells expression capacity of IκBα–gene (p_I^i) is assumed to be independent from TNF–receptor expression capacity, and also lognormal distributed, e.g.

$$p_I^i \sim \Lambda_I\big(\mu_{p_I}, \sigma_{p_I}\big) \ \forall i = 1(1)N, \tag{3.13}$$

with

	mean μ	**st. deviation σ**	**median**
$\Lambda_I(\mu_{p_I}, \sigma_{p_I})$	ln(6.5e-7)	0.4	7.0e-7

whereas the initial amount of IκBα mRNA of χ^i is given by

$$x_{Io}^i = \frac{p_I^i}{d_I}. \tag{3.14}$$

The distribution parameters (spread σ_{p_I} and mean μ_{p_I}) are estimated considering the experimental data, particularly cytotox assays.

These two independent extrinsic variables, TNF–receptor and IκBα gene expression, suffice to reproduce population heterogeneity of Kym-1 cells as observed in the experimental data.
In summary, a Kym–1 cell population is composed of N cells of the same type χ^i

$$\chi^i = \chi\big(\underline{\theta}^i, \underline{x}_o^i, u^i(t)\big) := \begin{cases} \dot{\underline{x}}^i(t) = f\big(\underline{x}^i(t), \underline{\theta}^i\big) + u^i(t) \\ \underline{x}^i(0) = \underline{x}_0^i \\ \underline{y}^i \end{cases},$$

subjected to the same (non–negative) TNF–input u(t):

$$\text{Pop} = \{\chi^1, \chi^2, ..., \chi^N \mid \text{N} \in \mathbb{N};\ u^i(t) = u(t)\ \forall i = 1(1)N\}.$$

The single cells χ^i differ in TNF–receptor expression capacity p_T^i and in IκBα–gene expression capacity p_I^i (and the corresponding initial values x_{To}^i and x_{Io}^i), e.g.

$$\chi^i = \chi\big(p_T^i, p_I^i, x_{To}^i, x_{Io}^i, u(t)\big),$$

whereas the remainder of the reaction rates and initial values are equal for all cells. The individual expression rates p_T^i and p_I^i are independent lognormal–distributed random variables,

$$p_T^i \sim \Lambda_T(\mu_{p_T}, \sigma_{p_T}),$$
$$p_I^i \sim \Lambda_I(\mu_{p_I}, \sigma_{p_I}),$$

with

	mean μ	**st. deviation σ**	**median**
$\Lambda_T(\mu_{p_T}, \sigma_{p_T})$	ln(2.19e-11)	0.31	2.3e-11
$\Lambda_I(\mu_{p_I}, \sigma_{p_I})$	ln(6.5e-7)	0.4	7.0e-7

For the initial concentrations x_{To}^i and x_{Io}^i holds

$$x_{To}^i = \frac{p_T^i}{d_T},\ x_{Io}^i = \frac{p_I^i}{d_I}.$$

3.5.2 Population Dynamics

The derived statistical model allows to calculate population–level dynamics. The population dynamics $\underline{y}_{Pop}(t)$ is obtained averaging and normalising the individual dynamics

$$\underline{y}_{Pop}(t) = \frac{1}{N}\sum_i \underline{x}^i(t). \tag{3.15}$$

As an example, Figure 3.4 shows the individual levels of active caspase 3 (1,3) and the normalised average population dynamic (2). Note that in this case, the average dynamic is a very poor indicator the individual cell behaves. The population model allows the adequate evaluation of population–wide data obtained by Western Blot analysis or EMSA for the purpose of parameter identification and model validation provided in Chapter 4.

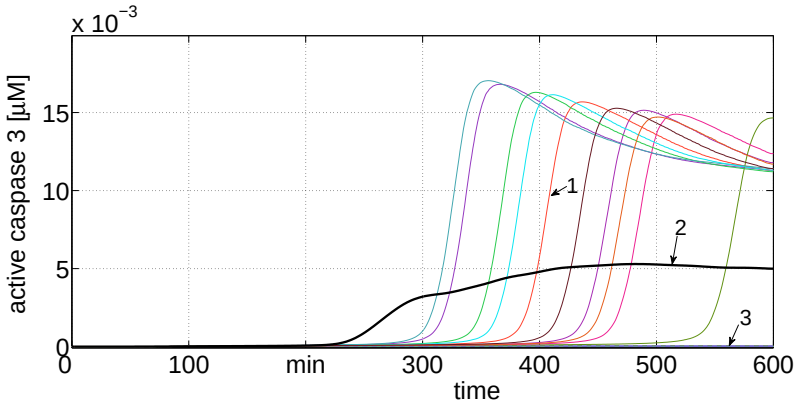

Figure 3.4: Individual and population dynamics of active Caspase 3. Individual cell responses are indicates with coloured lines, either apoptotic cells (1) or surviving cells (3). The normalised average population dynamics is indicated by the black line (2).

3.5.3 Characteristics Distributions

The individual characteristics y^i_{per}, y^i_{damp}, and y^i_{cd} are displayed with histograms tabulating the occurrence frequencies. Thereby, distributions of cell characteristics of the population are obtained, either in form of probability densities or in form of cumulative densities. The resulting distributions can be analysed with statistical methods, e.g. the mean, variance, and median can be calculated and compared with experimental data.

To illustrate the predictive power of the population model, the death distributions are calculated for a population composed of 1000 cells, see Fig. 3.5. The resulting distributions for a constant and pulse TNF–input (1.2 ng/ml) are displayed as histograms (see Fig. 3.5(a)) and corresponding cumulative distributions (Fig. 3.5(b)).

From the cumulative distributions, the cumulative density distributions are obtained, which can be compared with the cytotoxicity data, see Figure 3.5(b).

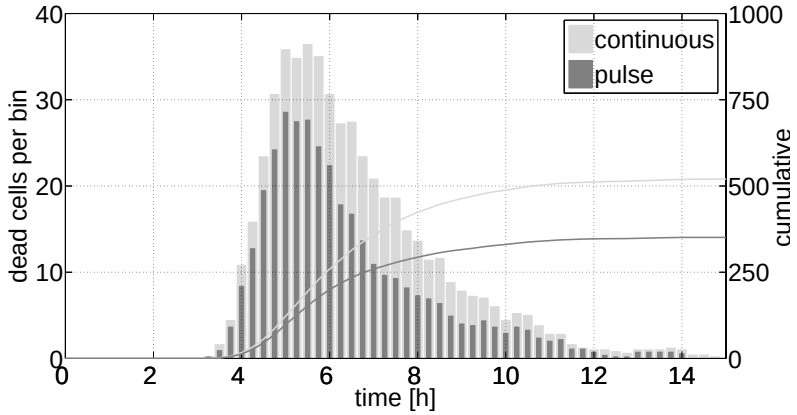

(a) Frequency histograms and corresponding cumulative distributions.

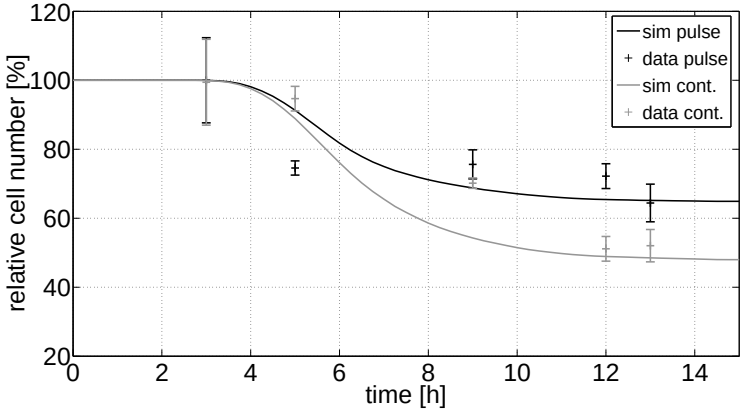

(b) Cumulative distribution in comparison with cytotoxicity data.

Figure 3.5: Death distributions of a population of 1000 cells for constant and 30 minutes pulse TNF–input (1.2 ng/ml).

3.6 Summary

Cell variability in general originates from inherent stochastics of the biochemical reactions and from extrinsic variations of cellular components; each cell has an individual history and at a given time point, cells of a population differ from one another in their cellular composition.

Relevant for the TNF–induced apoptosis signalling is the state of the cell at the time point of apoptosis induction, in particular its gene expression capacity. Cell–to–cell variations in gene expression capacity manifest individual composition such as the number of TNF–receptors of each cell; this in turn results in an individual cell behaviour and thus population heterogeneity.

Therefore, population heterogeneity is modeled considering cell–to–cell variations in gene expression capacity, particularly TNF–receptor expression and IκBα–gene expression. The expression capacities are assigned to a lognormal distribution, such that both expression rates are independent lognormal random variables. Gene expression within a single cell is constant over time. Thus, the model does not account for intrinsic stochastic of gene expression. A cell population is constituted by a (large) number of individual cells, all of which contribute in a different way to the overall population behaviour.

This statistical population approach allows to calculate population dynamics and the distributions of apoptosis characteristics such as cell death, period and dampening of NF–κB oscillations. Thereby, the evaluation of population–wide data obtained by cytotoxicity or EMSA is possible for the purpose of parameter identification and model validation.

Chapter 4

Analysis & Validation of the Population Model

In this chapter, the statistical population model is analysed and validated considering population–wide data. In the first section, the relative contributions of the variable expression rates are analysed with respect to population behaviour. In Section 4.2, population dynamics for NF–κB is investigated and compared with EMSA. In Section 4.3, the influence of the TNF–input on the cell population is analysed with respect to the apoptosis characteristics cell death (4.3.1), and period and dampening (4.3.3) of NF–κB N/C oscillations. The validation results concerning cell death distributions are presented in Section 4.3.2.

4.1 Influence of IκBα–gene Expression

The population model is based on the assumption of cell–cell variations in IκBαt and TNF–receptor expression capacity, whereas the individual expression rates are independent random variables assigned to a lognormal distribution $\Lambda_I(\mu_{p_I}, \sigma_{p_I})$ and $\Lambda_T(\mu_{p_T}, \sigma_{p_T})$ respectively.

The sensitivity analysis in Chapter 2, Section 2.2 showed that the apoptosis characteristics period, dampening and cell death are very sensitive with respect to IκBαt expression, but less sensitive with

respect to TNF–receptor expression.

The relative contribution of each variable expression rate on population heterogeneity is analysed with a correlation histogram, see Fig. 4.1. Hereby, the individual time points of cell death are tabulated with respect to the individual expression rates for a population of 2500 cells (subjected to a constant TNF–input 10 ng/ml).

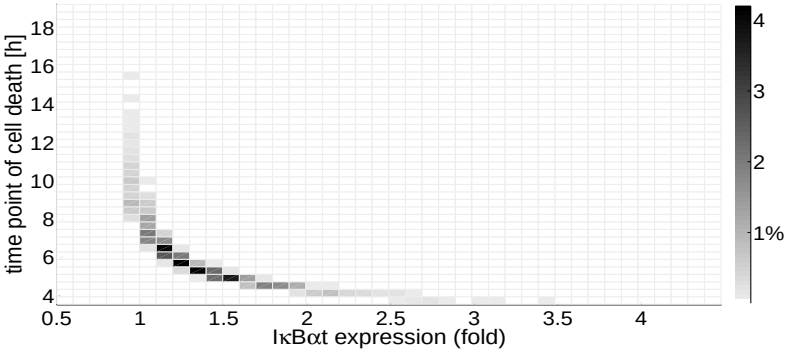

(a) IκBαt expression.

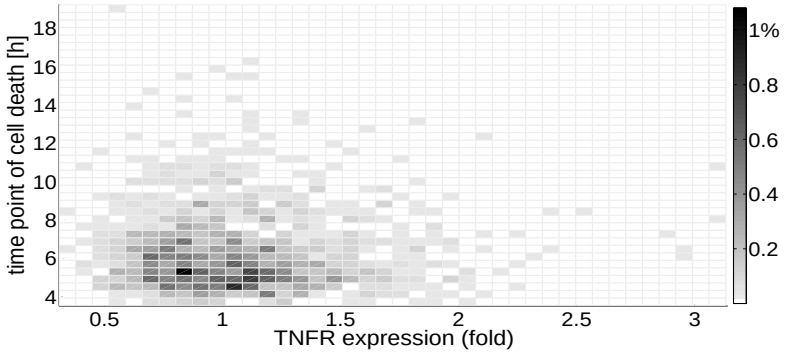

(b) TNF–R expression.

Figure 4.1: Correlation analysis of the relative contributions of the variable expression rates for cell death. Constant TNF–input of 10 ng/ml, population size: 2500 cells

Results IκBαt expression is strongly correlated with the time point of cell death 4.1(a), whereas TNF–receptor expression 4.1(b) is not correlated. Low rates of IκBαt expression cause slower NF–κB exported from the nucleus, which in turn rises the amount of produced inhibitors of caspases. High expression rates reduce NF–κB induced inhibitor production, thus lowering the inhibition potential of the cell.

Therefore, population heterogeneity with respect to cell death is dominated by cell–to–cell variations of IκBα–gene expression. This also holds for period and dampening of N–C NF–κB oscillations; the influence of cell–to–cell variations of IκBα–gene expression are significantly more momentous than variations of the TNF–receptor expression rate with respect to this apoptosis characteristics.

The influence of the shape parameters σ and μ of the distribution of IκBαt expression on the population heterogeneity are analysed with respect to the distribution of the NF–κB oscillation period in the next section.

4.1.1 Spread of IκBα mRNA Expression

Fig. 4.2(a) shows the probability density distribution for period characteristic for a low ($\sigma_{p_I} = 0.25$), medium ($\sigma_{p_I} = 0.40$), and high ($\sigma_{p_I} = 0.55$) value of the standard deviation at a constant μ_{p_I}. Increased σ results in a higher variance of the period characteristic of the entire population. Fig. 4.2(b) shows the corresponding cumulative density functions. Note that the median of the period distribution does not depend on the standard deviation.

4.1.2 Mean of IκBα mRNA Expression

In Fig. 4.3(a), the probability density distributions of the period characteristic are depicted for a low (/1.25), medium (1), and high (·1.25 with respect to reference parameter) value of μ_{p_I} at constant σ_{p_I}. Increasing μ results in a shift of the probability distributions, e.g. for a high μ the probability density distribution is shifted to the left, since higher expression levels of IκBα mRNA along with a faster period. Fig. 4.3(b) shows the corresponding cumulative density functions.

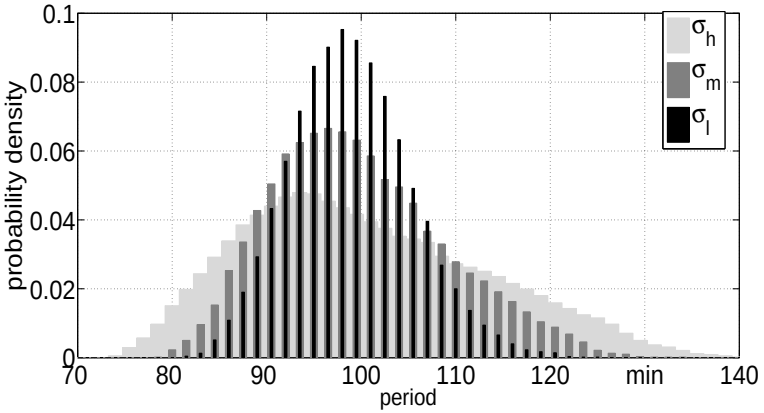

(a) Probability density functions.

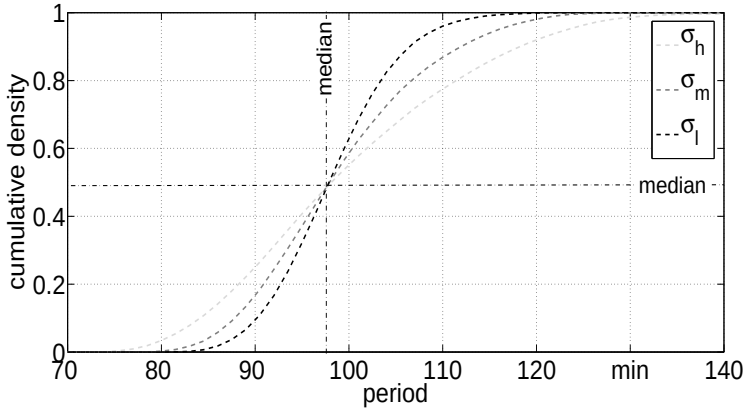

(b) Cumulative density functions.

Figure 4.2: Period characteristic distribution for low (σ_l), medium (σ_m) and high (σ_h) spread σ_{p_I} of $\Lambda_I(\mu_{p_I}, \sigma_{p_I})$.

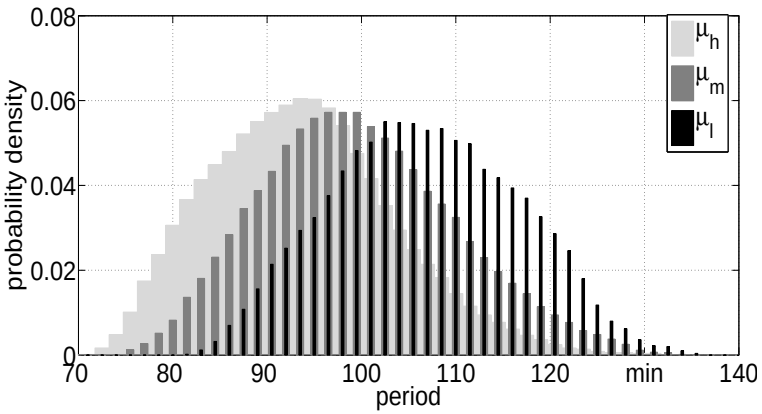

(a) Probability density functions.

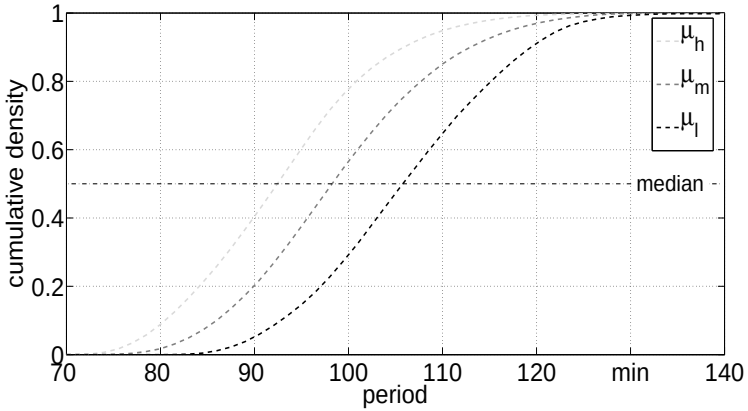

(b) Cumulative density functions.

Figure 4.3: Probability density function of period characteristic for low (μ_l), medium (μ_m) and high (μ_h) mean.

4.2 Population Dynamics of NF–κB

The derived statistical model allows to calculate population–level dynamics for the species concentrations. The population dynamics $\underline{y}_{Pop}(t)$ is obtained by averaging the individual dynamics as described in Equation (3.15).
Of particular interest is the calculation of the population dynamics with respect to the levels of nuclear NF–κB, since precise population–wide data is available for different TNF–inputs (IZI Stuttgart).

4.2.1 NF–κB Oscillations

TNF–induced nucleus–cytoplasm oscillations in NF–κB localisation have been reported and measured at single cell level. The average period for contant stimulation is about 100 minutes (Nelson et al. [2004]). Due to single cell variability, these oscillations may be washed out in population–average measurements, at least for SK–N–AS cells (see Figure 3.1).

This population effect can be reproduced with the population model, see Figure 4.4. Single cell dynamics of four arbitrary cells are indicated by coloured lines, whereas the average population dynamics is indicated by the black line.

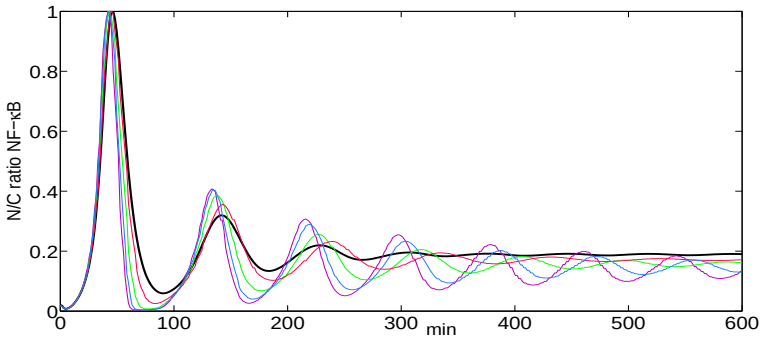

Figure 4.4: Single cell and population dynamic of N–C NF–κB oscillations. Population average dynamics is indicated by the black line (corresponding to 1000 cells). Colored lines indicate arbitrarily chosen single cells.

4.2.2 TNF Influence on NF–κBn Dynamics

The activation of the nuclear NF–κB is input dependent, see Fig. 4.5 and 4.6. Activation of NF–κB is the faster the higher the TNF dose. For a continuous TNF input (Fig. 4.5(a)), a constant level of nuclear factor NF–κBn is reached after about 6 hours, whereas for the 30 min. pulse input (Fig. 4.5(b)) the level of NF–κB decreases to zero. Remarkably, only for high pulse levels of TNF (> 3 ng/ml), a second

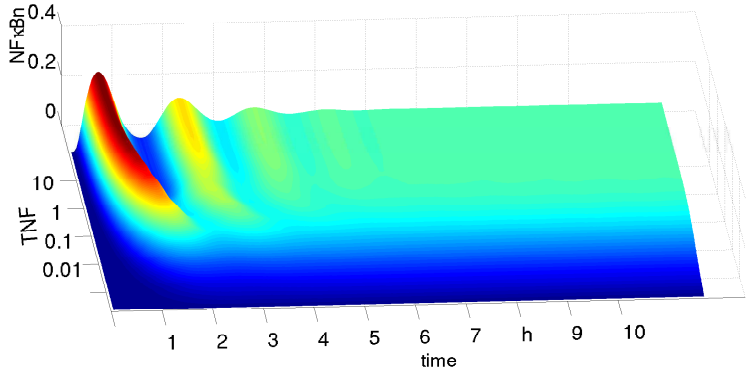

(a) Permanent stimulation.

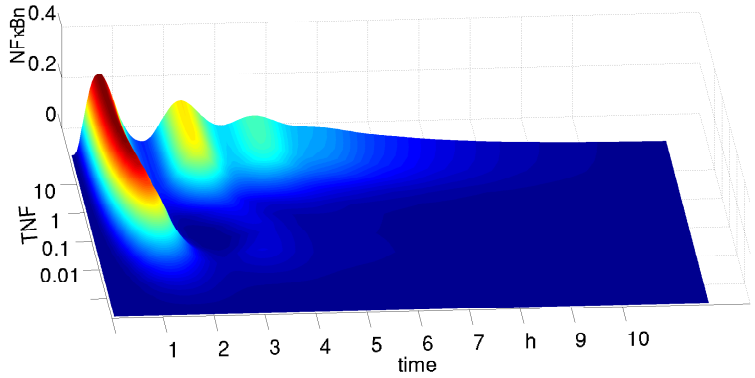

(b) 30 min pulse stimulation.

Figure 4.5: Influence of TNF-amplitude on NF-κB activity.

NF–κB peak occurs.

Since the amount of NF–κB in the cell is limited, the amplitude of the first NF–κBn peak saturates for high TNF–levels (> 1 ng/ml).

The influence of the pulse duration is shown for a TNF–amplitude of 3 ng/ml in Fig. 4.6. Activation velocity does not depend on pulse length.

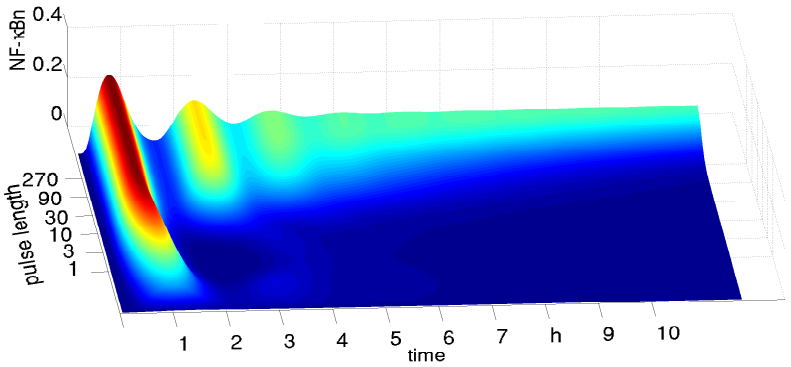

Figure 4.6: Influence of pulse duration on the level of nuclear NF-κB. TNF-pulse input at 3 ng/ml.

4.2.3 Validation Results: Levels of NF–κBn

The population dynamic of nuclear NF–κB in KYM–1 cells have been measured with EMSA for different TNF–inputs. In the following, the population model simulations and the measurements are compared.

Low TNF–input

For the low TNF–input, the population model is in good accord with the EMSA data, see Figure 4.7. The model captures the differences of continuous and pulse input.

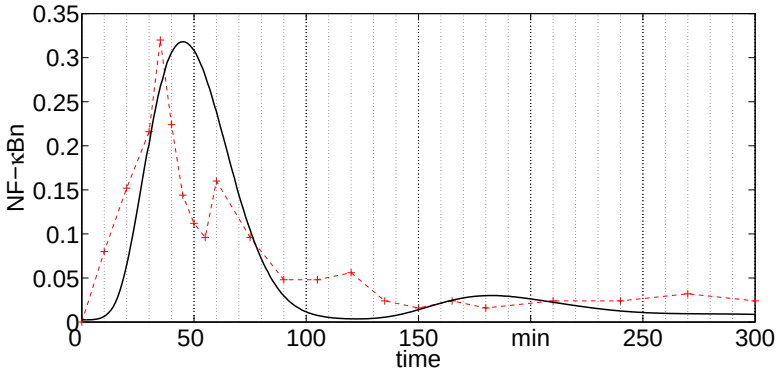

(a) 30 min pulse stimulation.

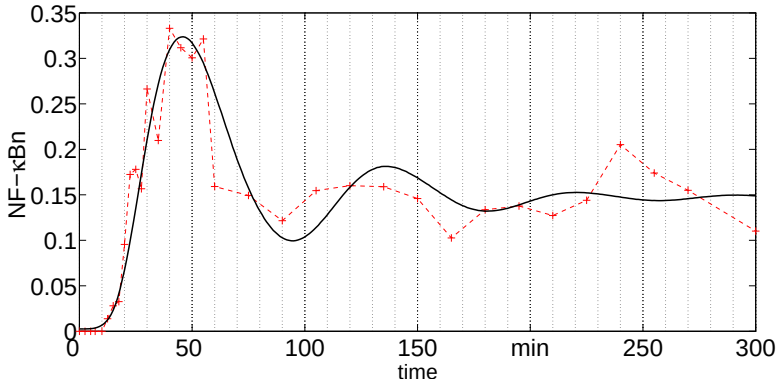

(b) Permanent stimulation.

Figure 4.7: Level of NF-κBn for low TNF–input (0.3 ng/ml).

High TNF–input

Also for a very high TNF–amplitude of 10 ng/ml, the population model in in good accord with the experimental data, see Figure 4.8.

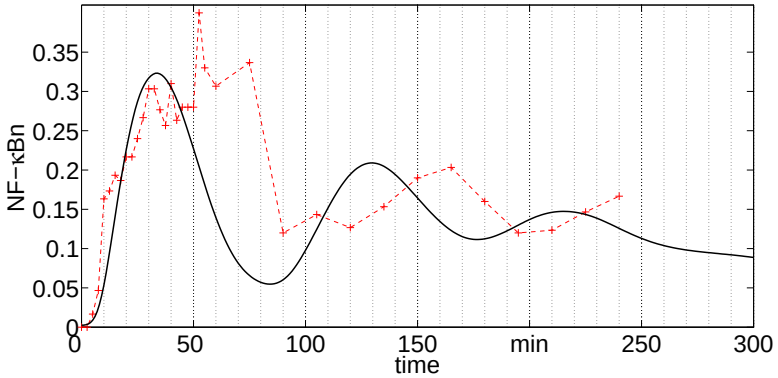

(a) 30 min pulse stimulation.

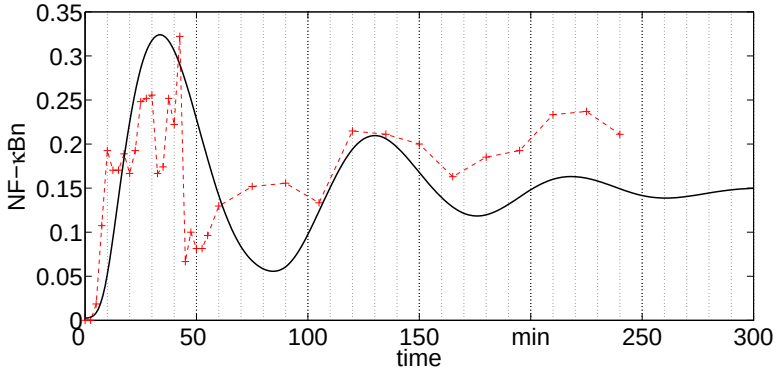

(b) Permanent stimulation.

Figure 4.8: Level of NF-κBn for high TNF–input (10 ng/ml).

Start Dynamics

The dose dependency of the velocity of NF–κBn activation is depicted in Fig. 4.9. Because there are only three data points for each amplitude (at 7.5, 15, and 30 min), quantitative comparison with population model dynamics is not reliable. However, qualitatively the dose-dependency is captured very well.

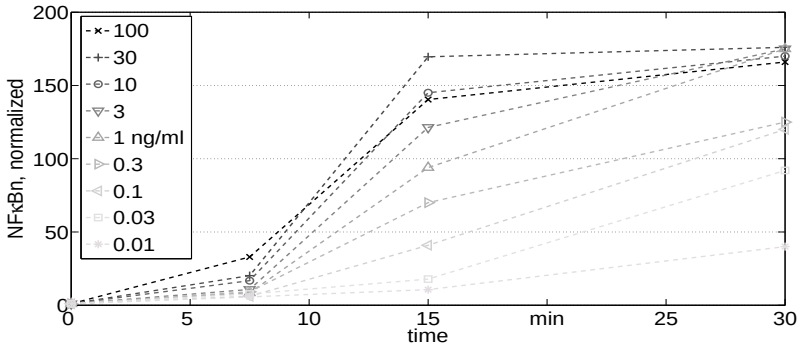

(a) EMSA data for level of NF–κBn at different TNF–amplitudes.

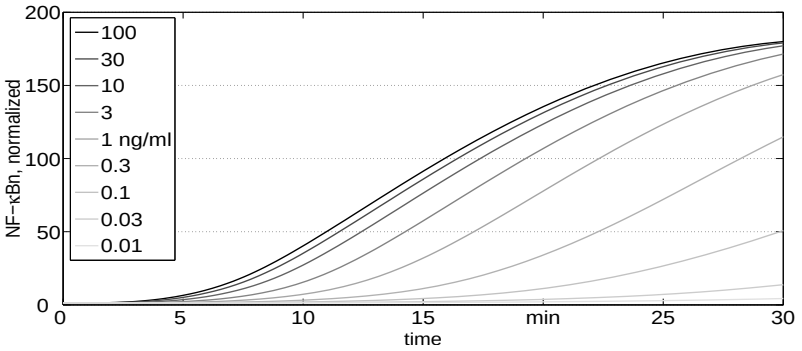

(b) Calculated population dynamics.

Figure 4.9: Level of NF-κBn for 30 min TNF–input at different doses.

4.3 TNF Influence on Apoptosis Characteristics

4.3.1 Cell Death

The population model allows to calculate probability densities and corresponding cumulative distributions for apoptosis cell death characteristic y_{cd}. The probability densities are represented as histograms. Fig. 4.10 shows the dose dependency of cell death with respect to continuous (4.10(a)) and 30 min pulse (4.10(b)) TNF–input.

Results Cell mortality is dose dependent. For moderate stimuli ($0.1 < \text{TNF} < 10$ ng/ml), the higher the TNF–amplitude the higher the death probability. However, increasing the TNF–amplitudes (TNF > 10 ng/ml) has little additional effect on mortality probability. For low TNF concentrations (< 0.1 ng/ml), neither a continuous nor a pulse input induces significant cell apoptosis at population level.

The mean time point of death is dose dependent. The lower the TNF–amplitude the later cells die. This trend is in particular obvious for continuous TNF–input. A possible explanation for this is that the inhibitors of caspases delay caspase activation. For low TNF–doses, caspase activation triggering signal (late Complex 2) is relatively low, such that the continuous production of inhibitors via NF–κB delays or successfully inhibits caspase activation.

Some cells survive even for very high TNF–amplitudes, see Figure 4.11. Cell survival is correlated with the expression rate of IκBα mRNA. Cells with low IκBα–gene expression rates produce large amount of caspase inhibitors, such that caspase activation is inhibited.

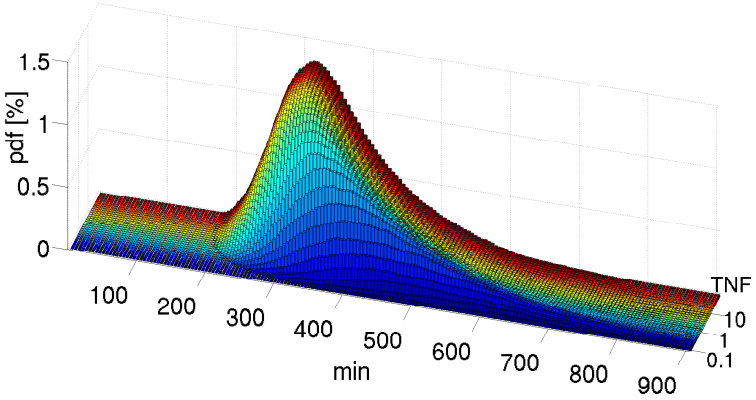

(a) Permanent stimulation.

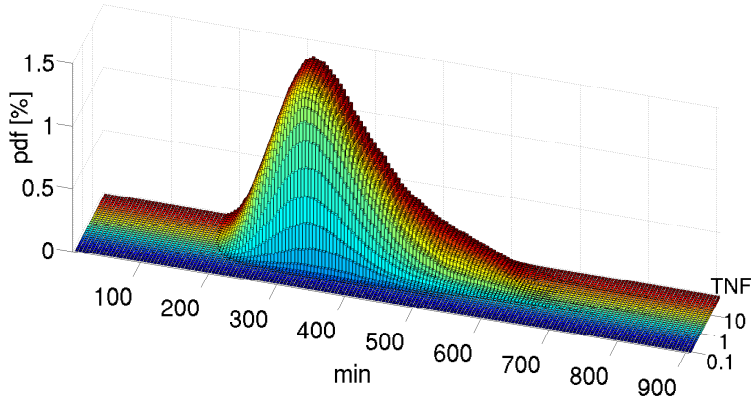

(b) 30 min pulse stimulation.

Figure 4.10: Probability density functions of cell mortality for different TNF–amplitudes. TNF in [ng/ml].

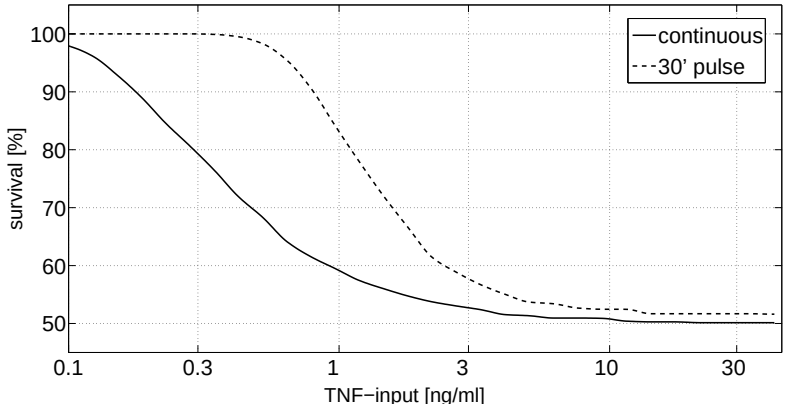

Figure 4.11: Relative cell survival rates for continuous and pulse TNF–input.

4.3.2 Validation Results: Cytotoxicity

The population responses to different TNF–inputs have been measured in cytotoxicity assays considering Kym–1 cells treated with serial dilutions of TNF–α (Schliemann et al. [2007]). The data is compared with population model simulations in Fig. 4.12. The population model captures dose dependency for pulse TNF input (4.12(a)) and for constant input (4.12(b)). The model predictions are qualitatively in good accord with the experimental data, though for high TNF amplitudes (> 3 ng/ml) and constant input the simulation results deviate from the data, which might be explained by possible ointerferences of the mitochondrial apoptosis pathway at high TNF doses. Also, the cytotoxity data might be biased by a TNF-alpha induced proliferation, in particular for low TNF amplitudes.

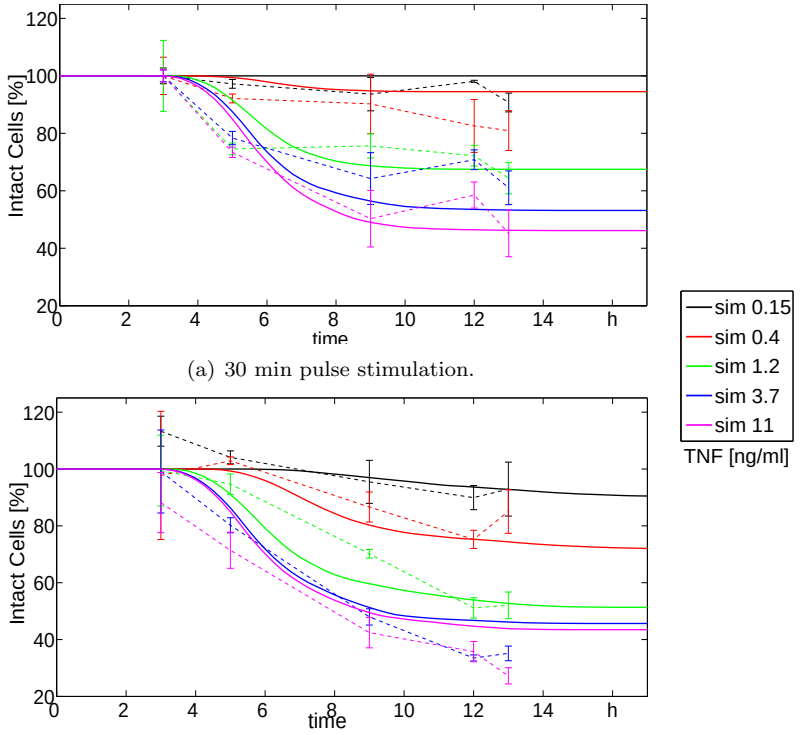

(a) 30 min pulse stimulation.

(b) Permanent stimulation.

Figure 4.12: Cytotoxicity data and cumulative mortality density at different TNF–inputs. Full lines indicate the simulated population responses, dashed lines and errorbars the experimental data.

4.3.3 Period and Dampening of NF–κB Oscillations

In the following, the distributions of period and dampening characteristics are evaluated for a cell population (size 1000 cells) with respect to a low (0.1 ng/ml), a medium (1 ng/ml) and high (10 ng/ml) constant TNF–input. The histograms 4.13(a) and 4.14(a) show the calculated probability densities for the characteristics; Fig. 4.13(b) and 4.14(b) show the corresponding cumulative density distributions.

Results Period and dampening of NF–κB oscillations are little sensitive with respect to the TNF–amplitude. The median period varies only from 96 min (0.1 ng/ml) to 98 min (10 ng/ml); also the shape of the distributions does not vary significantly with the TNF–amplitude, though the spread of dampening distribution (Fig. 4.14(a)) increases for low TNF–amplitude.

The computed median period for 10 ng/ml (about 98 min) matches the experimental observations of Nelson et al. [2004] observing an average period of about 100 minutes.

Dampening and period are correlated in the simulation, see Figure 4.15. An experimental validation would be interesting.

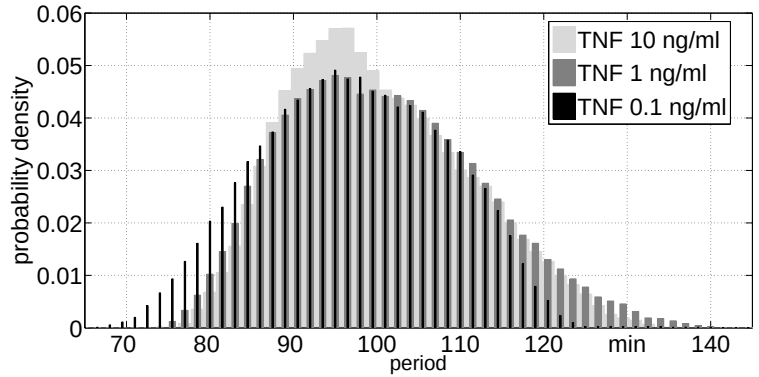

(a) Probability density functions.

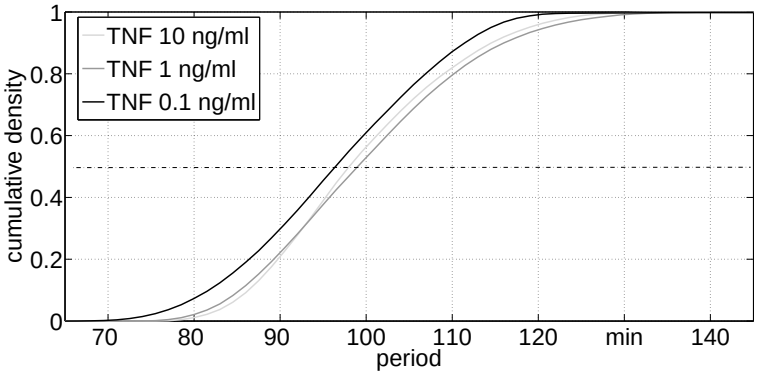

(b) Cumulative density functions.

Figure 4.13: Distribution of NF–κB period for different TNF amplitudes.

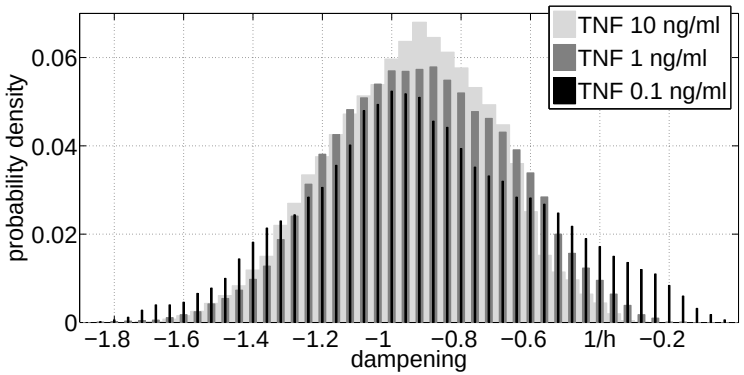

(a) Probability density functions.

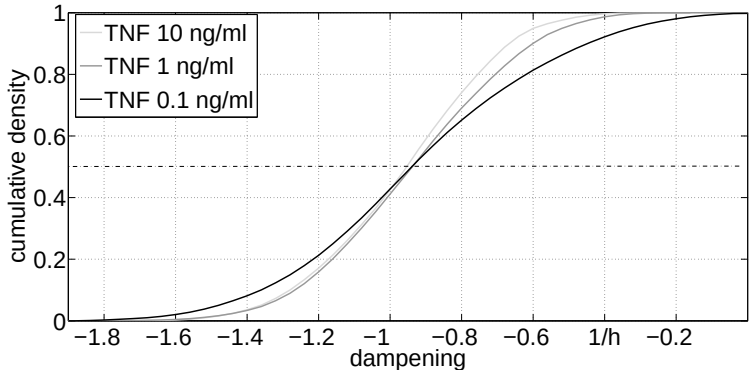

(b) Cumulative density functions.

Figure 4.14: Distribution of NF–κB dampening for different TNF amplitudes.

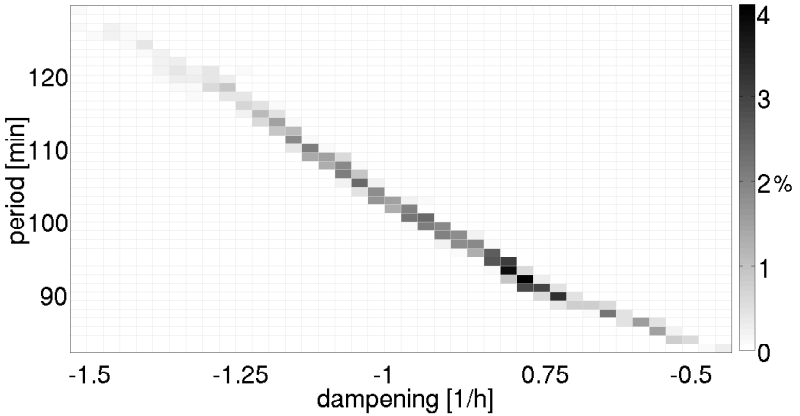

Figure 4.15: Correlation of period and dampening of NF-κB oscillations within a cell population; constant TNF–input (10 ng/ml).

4.4 Conclusions

The population model of TNF–induced apoptosis is based on cell–to–cell variations of the gene expression rates of TNF–receptor and IκBα mRNA. Analysis of the relative contributions of each expression rate revealed that mainly latter contributes to population heterogeneity in apoptosis characteristics.

The population model enables to compute population dynamics for species concentrations and thus allows to evaluate and to compare population–wide measurements such as EMSA or Western blotting for the purpose of parameter identification and model validation. The population dynamics of nuclear NF–κB are compared with EMSA. The population model is in good accord with the experimental data for low (0.3 ng/ml) and high (10 ng/ml) TNF–input. The model captures the differences of constant and pulse inputs and reliably reproduces dose dependency with respect to velocity of activation of nuclear NF–κB.

Via the computation of the cell death distributions, the cytotoxicity assays can be evaluated. Models predictions match the experiments very well. Dose dependency is captured for pulse TNF–inputs

as well as for constant TNF–inputs, though for high TNF–amplitudes (> 3 ng/ml) and constant input the simulation results deviate from the data.

The median period of N–C NF–κB oscillations (about 98 min) matches the single cell studies of Nelson et al. [2004] observing an average period of about 100 minutes.

Overall, the TNF–induced apoptosis population model is qualitatively and quantitatively in good accord with the available experimental data. Dose–dependency and the differences of pulse and constant TNF–input are captured for levels of nuclear NF–κB and cell death. An experimental validation of the model prediction concerning insensitivity of N–C NF–κB dampening and period with respect to TNF–dose would be very interesting.

Chapter 5

Discussion, Summary and Outlook

In systems biology, cellular processes are often described as biochemically structured networks in form of ordinary differential equations. These single–cell models contain a significant amount of biological details in form of networks topology and parameters, and are of great advantage for the purpose of a better understanding of the regarded process. Insights into systems properties and behaviour can be obtained by mathematical analysis, e.g. simulation studies or local parameter sensitivity and bifurcation analysis.

However, most of biological applications also require an understanding of cellular processes at cell population level, in the first place the evaluation of bulk–cell data for the purpose of parameter identification and model validation. Cell populations are heterogeneous systems being composed of topological identical, nevertheless individual cells due to differences in composition from cell–to–cell and over time within a single cell. Thus, cell populations are characterised by an additional level of complexity owing to cell variability. The general and hence hard question of how can cell variability and thus population heterogeneity be accurately described cannot be treated in general, it depends on the regarded cellular process and the cell type.

Cell variability in TNF–induced apoptosis signalling in general

may arise from inherent stochastic of the network reactions and from extrinsic fluctuations of cellular components. As outlined in Chapter 3, the influence of inherent stochastic is small, whereas apoptotic cell behaviour significantly depends on the initial state of the cell at the time point of apoptosis induction. Since cell–to–cell variations of cellular compounds such as the TNF–receptor have been determined experimentally, a natural assumption is that cell population heterogeneity in TNF–induced apoptosis is driven by cell–to–cell variations. These variations presumably originate from variations in gene expression, and can be approximated by the skewed distributions.

Therefore, population heterogeneity of a Kym–1 cell population is modeled considering cell–to–cell variations in gene expression capacity in otherwise identical cells, particularly TNF–receptor expression and IκBα–gene expression. The expression capacities are lognormal distributed amongst the cells of the population, but constant within a single cell.

This statistical population approach allows to calculate population dynamics and the distributions of apoptosis characteristics such as cell death, period and dampening of NF–κB oscillations. The population model is used to evaluate bulk–cell data obtained by cytotoxicity and EMSA to reestimate the model parameters and to validate the TNF–induced apoptosis model.

Overall, the TNF–induced apoptosis model is is qualitatively and quantitatively in good accord with the single–cell and population–level experimental data. The model captures TNF–dose dependency and the differences of constant and pulse inputs with respect to levels of nuclear NF–κB and cell death, and cell exhibits NF-κB nucleus-cytoplasmic oscillations with a typical period of approx. 100 minutes for five cycles. An experimental validation of the model prediction such as insensitivity of N–C NF–κB oscillation dampening and period with respect to TNF–dose would be very interesting.

Outlook

This thesis aimed to contribute to the development of a predictive apoptosis model. Considering the large number of model parameters, more quantitative data is desirable and also necessary. The most sensitive reaction rates should be experimentally determined. To facilitate future refinement of model parameters regarding large sets of quantitative experimental data, the formulation of the optimal identification problem would be very helpful but challenging. Hereby, identifiably analysis and experimental design can help to direct measurements with high informative values.

The analysis could also be extended and complemented with a robustness analysis considering bifurcation–based robustness measures, e.g. Ma and Iglesias [2002].

Another interesting future direction may be the incorporation of the intrinsic apoptosis pathway. Hereby, truncated Bid (t–Bid) interfaces the current TNF–induced apoptosis model with the mitochondrial pathway. Such an extended model in combination with appropriate experimental data may provide insight in the differences of Type I and II cells.

Bibliography

A Ashkenazi and VM. Dixit. Death receptors: signaling and modulation. *Science*, 281:1305–8, 1998.

EZ Bagci, Y Vodovotz, TR Billiar, GB Ermentrout, and I Bahar. Bistability in apoptosis: Roles of Bax, Bcl-2, and mitochondrial permeability transition pores. *Biophysical Journal*, 90:1546–1559, 2006.

A Becskei and L Serrano. Engineering stability in gene networks by autoregulation. *Nature*, 405:590–593, 2000.

M Bentele, I Lavrik, M Ulrich, S Stör, DW Heermann, H Kalthoff, PH Krammer, and R Eils. Mathematical modeling reveals threshold mechanism in CD95–induced apoptosis. *The Journal of Cell Biology*, 166(6):839–51, 2004.

KH Cho, SY Shin, W Kolch, and O Wolkenhauer. Experimental design in systems biology, based on parameter sensitivity analysis using a Monte Carlo method: A case study for the TNF-α–mediated NF-κB signal transduction pathway. *Simulation*, 79(12):726–739, 2003.

A Colman-Lerner, A Gordon, E Serra, T Chin, O Resnekov, D Endy, CG Pesce1, and R Brent. Regulated cell-to-cell variation in a cell-fate decision system. *Nature*, 437:699–706, 2005.

JD Crawford. Introduction to bifurcation theory. *Reviews of Modern Physics*, 63(4):991–1037, 1991.

SK Dower and EE Qwarnstrom. Signalling networks, inflammation and innate immunity. *Biochemical Society Transactions*, 31:1462–1471, 2003.

T Eissing, H Conzelmann, ED Gilles, F Allgöwer, E Bullinger, and P Scheurich. Bistability analyses of a caspase activation model for receptor–induced apoptosis. *The Journal of Biological Chemistry*, 279(35):36892–7, 2004.

T Eissing, S Waldherr, F Allgöwer, P Scheurich, and E Bullinger. Response to bistability in apoptosis: Roles of Bax, Bcl-2, and mitochondrial permeability transition pores. *Biophysical Journal*, 92: 3332–3334, 2007.

MB Elowitz, AJ Levine, ED Siggia, and PS Swain. Stochastic gene expression in a single cell. *Science*, 297(5584):1183–6, 2002.

M Fussenegger, JE Bailey, and J Varner. Mathematical model of caspase function in apoptosis. *Nature Biotechnology*, 18:768–775, 2000.

S Gaudet, KA Janes, JG Albeck, EA Pace, DA Lauffenburger, and PK Sorger. A compendium of signals and responses triggered by prodeath and prosurvival cytokines. *Molecular and Cellular Proteomics*, 4(10):1569–1590, 2005.

C Haass. Apoptosis. Dead end for neurodegeneration? *Nature*, 399: 204–207, 1999.

F Hayot and C Jayaprakash. NF–κB oscillations and cell-to-cell variability. *Quantitative Biology*, pages 1–14, 2005.

MA Henson, D Müller, and M Reuss. Cell population modelling of yeast glycolytic oscillations. *Biochemical Journal*, 368(2):433–46, 2002.

A Hoffmann, A Levchenko, ML Scott, and D Baltimore. The IκB–NF-κB signaling module: Temporal control and selective gene activation. *Science*, 298(5596):1241–1245, 2002.

JD Kearns, S Basak, SL Werner, CS Huang, and A Hoffmann. IκBϵ provides negative feedback to control NF-κB oscillations, signaling dynamics, and inflammatory gene expression. *The Journal of Cell Biology*, 173(5):659–64., 2006.

S Legewie, N Blüthgen, and H Herzel. Mathematical modeling identifies inhibitors of apoptosis as mediators of positive feedback and bistability. *PLoS Computational Biology*, 2(9):1061, 2006.

JM Levsky, SM Shenoy, RC Pezo, and RH Singer. Single–cell gene expression profiling. *Science*, 297:836–840, 2002.

E Limpert, W Stahel, and M Abbt. Log-normal distributions across the sciences: Keys and clues. *Bioscience*, 51(5):341–352, 2001.

T Lipniacki, P Paszek, AR Brasier, B Luxon, and M Kimmel. Mathematical model of NF-κB regulatory module. *Journal of Theoretical Biology*, 228(2):195–215, 2004.

L Ma and PA Iglesias. Quantifying robustness of biochemical network models. *BMC Bioinformatics*, 3:38, 2002.

NV Mantzaris. Single-cell gene-switching networks and heterogeneous cell population phenotypes. *Computers and Chemical Engineering*, 29:631–643, 2005.

NV Mantzaris. From single-cell genetic architecture to cell population dynamics: Quantitatively decomposing the effects of different population heterogeneity sources for a genetic network with positive feedback architecture. *Biophysical Journal*, 92:4271–4288, 2007.

JC Mar, R Rubio, and J Quackenbush. Inferring steady state single-cell gene expression distributions from analysis of mesoscopic samples. *Genome Biology*, 7(12):R119.1–12, December 2006.

ER McDonald and WS El-Deiry. *The Proceedings of the National Academy of Sciences USA*, 101:6170–75, 2004.

O Micheau and J Tschopp. Induction of TNF receptor I-mediated apoptosis via two sequential signaling complexes. *Cell*, 114:181–190, 2003.

S Nagata. Apoptosis by death factor. *Cell*, 88:355–65, 1997.

DE Nelson, AE Ihekwaba, M Elliott, JR Johnson, CA Gibney, BE Foreman, G Nelson, V See, CA Horton, DG Spiller, et al. Oscillations in NF-κB signaling control the dynamics of gene expression. *Science*, 306(5696):704–8, 2004.

S Ramsey, A Ozinsky, A Clark, KD Smith, P de Atauri, V Thorsson, D Orrell, and H Bolouri. Transcriptional noise and cellular heterogeneity in mammalian macrophages. *Philosophical Transactions of the Royal Society B: Biological Sciences*, 361:495–506, 2006.

P. Rangamani and L. Sirovich. Survival and apoptotic pathways initiated by TNF-α: Modeling and predictions. *Biotechnology and Bioengineering*, DOI 10.1002/bit. 21307, 2006.

JM Raser and EK O'Shea. Noise in gene expression: origins, consequences, and control. *Science*, 309(5743):2010–3, 2005.

M Rehm, HJ Huber, H Dussmann, and JHM Prehn. Systems analysis of effector Caspase activation and its control by X–linked inhibitor of apoptosis protein. *EMBO Journal*, 25:4338–4349, 2006.

N Rosenfeld, JW Young, U Alon, PS Swain, and MB Elowitz. Gene regulation at the single-cell level. *Science*, 307(5717):1962–5, 2005.

M Schliemann. Mathematische Modellierung des TNF–induzierten apoptotischen und antiapoptotischen Signaltransduktionsweges in Säugerzellen. *Diploma Thesis, IZI Stuttgart*, 2006.

M Schliemann, T Eissing, P Scheurich, and E Bullinger. Mathematical modelling of TNF-induced apoptotic and anti-apoptotic signalling pathways in mammalian cells based on dynamic and quantitative experiments. *Proceedings of 2nd Conference on the Foundations of Systems Biology in Engineering (FOSBE), Stuttgart*, pages 213–8, 2007.

Monica Schliemann. Unpublished data. *IZI Stuttgart*, 2007.

K Sillitoe, C Horton, DG Spiller, and MR White. Single-cell time-lapse imaging of the dynamic control of NF-κB signalling. *Biochemical Society Transactions*, 35:263–6, 2007.

A Strasser, L O'Connor, and VM Dixit. Apoptosis signaling. *Annual Review Biochememistry*, 69:217–45, 2000.

SH Strogatz. Nonlinear dynamics and chaos. *Reading, MA: Addison-Wesley*, 1994.

PS Swain, MB Elowitz, and ED Siggia. Intrinsic and extrinsic contributions to stochasticity in gene expression. *The Proceedings of the National Academy of Sciences USA*, 99(20):12795–12800, 2002.

LS Weinberger, JC Burnett, JE Toettcher, AP Arkin, and DV Schaffer. Stochastic gene expression in a lentiviral positive-feedback loop: HIV–1 tat fluctuations drive phenotypic diversity. *Cell*, 122: 169–182, 2005.

W Yang, LM Rozan, ER McDonald, A Navaraj, JJ Liu, W Matthew, EM Wang, DT Dicker, and WS El-Deiry. CARPs are Ubiquitin ligases that promote MDM2-independent p53 and Phospho-p53ser20 degradation. *The Journal of Biological Chemistry*, 282(5):3273–81, 2007.

H Yue, M Brown, J Knowles, H Wang, DS Broomhead, and DB Kell. Insights into the behaviour of systems biology models from dynamic sensitivity and identifiability analysis: a case study of an NF-κB signalling pathway. *Molecular Biosystems*, 2:640–649, 2006.

Appendix

Model Parameter Adaptation

Reception Module

Reaction	sym-bol	old [μM]	new [μM]	factor
Transition Extern→Intern				
Cex→0	ka(3)	1	0.4	÷2.5
Cex→C0 + Cex	ka(4)	2e4	3.5e4	×1.75
▷ *lower up–concentration extern → intern (receptor dimerisation); important for NF–κBn offset at high pulse stimulus*				
A20				
A20 + C1→A20a + C1	ka(8)	2.5e-1	2.5	×10
▷ *making A20 feedback effective*				
Binding FLIP – C2				
FLIP + C2→C2∼FLIP	ka(22)	2.5e-5	3e-5	×1.2
▷ *making FLIP–inhibition more effective*				

Table 5.1: Changes in the reception module.

NF–κB Module

Reaction	sym-bol	old [μM]	new [μM]	factor
IKK related changes				
IKKn + C1→IKKa + C1	ka(25)	2.5e-3	0.75	×300
▷ *adaptation of the logical Lipniacki-input (C1=1) to "real" C1∼0.001*				
IKKa→IKKi	ka(26)	1.5e-3	2.3e-2	×15
▷ *influences period and first–peak time of NF–κB*				
IKKa + IκBα ∼NF–κB→ IKKa∼IκBα ∼NF–κB	ka(34)	1	1.9	×1.9
IKKa∼IκBα ∼NF-κB→ IKKa + NFκB	ka(35)	0.1	2.5e-3	÷40
▷ *very important for NF-κBn offset at permanent stimulation*				
Degradation Rates				
IκBαt →0	ka(44)	4e-4	1e-3	×2.5
▷ *influences NF-κBn amplitude*				
Association Rates				
IκBα + NF-κB→ IκBα ∼NF-κB	ka(33)	0.5	0.165	÷3
▷ *influences NF-κBn oscillations, e.g. amplitudes, period*				

Reaction	sym-bol	old μM	new μM	factor
Expression Rates				
NF-κBn →NFκBn+IκBαt	ka(42)	5e-7	6.5e-7	×1.3
▷ *period, dampening, amplitudes*				
IκBαt →IκBα+IκBαt	ka(43)	0.5	0.75	×1.5
▷ *amplitudes, period*				
NF-κBn →IAPt + NF-κBn	ka(53)	7e-6	7e-7	÷10
▷ *pulse-permanent distinction*				
0 →IAP	ka(56)	1e-5	2.8e-5	×2.7
NF-κBn →FLIPt + NFκBn	ka(57)	4.4e-4	1.8e-4	÷2.5
0 →FLIP	ka(60)	8.1e-5	1.6e-4	×2
Transport: ratio volume cytoplasm (V_{cy}) to nucleus (V_{nu}): $V_{cy}/V_{nu} = 2.5$				
NF-κB→0	ka(36)	2.5e-3	1.5e-3	÷1.66
NF-κB→NF-κBn+NF-κB	ka(37)	1.3e-2	3.8e-3	÷3
IκBα →0	ka(46)	1e-3	2.2e-3	×2.2
IκBα →IκBαn + IκBα	ka(47)	5e-3	5e-3	1
IκBαn→0	ka(46)	1e-3	2e-3	×2
IκBαn→IκBα + IκBαn	ka(47)	5e-3	5e-3	1
IκBαn∼NF-κBn→0	ka(51)	5e-2	2.5e-2	÷2
IκBαn∼NF-κBn→ IκBα ∼NF-κB + IκBαn∼NF–κBn	ka(52)	1e-2	1e-2	1

Table 5.2: Changes in the NF-κB signalling module.

Caspase Module

Reaction	sym-bol	old μM	new μM	factor
Stability				
C8a+C3→C8a+C3a	ka(63)	0.1	0.04	÷2.5
C3a+C8→C8a+C3a	ka(64)	0.1	0.04	÷2.5
C8a→0 ▷ *CARP substitution*	ka(72)	9.7e-5	7.7e-4	×8
Bistability				
0⟷C8	ka(61)	1.4e-5	1.8e-5	×1.3
	kd(61)	6.5e-5	8.5e-5	×1.3
0⟷C3	ka(62)	2.3e-6	3e-6	×1.3
	kd(62)	6.5e-5	8.5e-5	×1.3
Adaptation				
C8+C2→C8a+C2	ka(63)	3e-2	7.5e-3	÷4

Table 5.3: Changes in the caspase module.

Model Summary

Reactions List

Here, a complete list of reactions is provided. The reactions form the basis of the mathematical apoptosis model assuming mass action for reaction dynamics. All parameter changes with respect to Schliemann [2006] are pointed out in the column "remark".

N	Reaction	value	unit	remark
Reception Module				
1	0→ TNFR	2.2e-11	$\frac{\mu M}{s}$	3000 Receptors per cell
	0← TNFR	9.2e-5	$\frac{1}{s}$	
2	TNF + TNFR→ Cex	1.8e1	$\frac{1}{\mu M s}$	÷2.5
	TNF + TNFR← Cex	3.5e-4	$\frac{1}{s}$	×1.8
3	Cex→ 0	0.4	$\frac{1}{s}$	
4	Cex→ C0 + Cex	3.5e4	$\frac{1}{s}$	
5	0→ RIP	1.1e-6	$\frac{\mu M}{s}$	
	0← RIP	1.7e-4	$\frac{1}{s}$	
6	RIP + C0→ Czw0	1.3	$\frac{1}{\mu M s}$	
7	Czw0→ C1	1.0e4	$\frac{1}{s}$	
8	A20+C1→ A20a+C1	2.5	$\frac{1}{\mu M s}$	×10
9	A20a→ 0	3e-4	$\frac{1}{s}$	
10	C1→ Czw1	1.5e-3	$\frac{1}{s}$	
11	C1→ 0	7.0e-6	$\frac{1}{s}$	
12	C0→ Czw1	1.5e-6	$\frac{1}{s}$	
13	C0→ 0	7.0e-6	$\frac{1}{s}$	
14	Czw1→ Czw2	1.5e-3	$\frac{1}{s}$	
15	Czw2→ Czw3	1.5e-3	$\frac{1}{s}$	
16	Czw3→ Czw4	1.5e-3	$\frac{1}{s}$	
17	Czw4→ Czw5	1.5e-3	$\frac{1}{s}$	

18	Czw5→ Czw6	1.5e-3	$\frac{1}{s}$	
19	Czw6→ C2	1.5e-2	$\frac{1}{s}$	
20	C2→ 0	7e-4	$\frac{1}{s}$	
21	C3a + RIP→ C3a	1e-3	$\frac{1}{\mu Ms}$	
22	C2 + FLIP→ C2∼FLIP	3.0e-5	$\frac{1}{\mu Ms}$	×1.2
	C2 + FLIP← C2∼FLIP	1.8e-6	$\frac{1}{s}$	
23	C2∼FLIP→ 0	1.4e-2	$\frac{1}{s}$	
24	C3a + FLIP→ C3a	1.5	$\frac{1}{\mu Ms}$	
Antiapoptotic Module				
25	0→ IKKn	2.5e-5	$\frac{\mu M}{s}$	
	0← IKKn	1.3e-4	$\frac{1}{s}$	
26	IKKn + C1→ IKKa + C1	7.5e-1	$\frac{1}{\mu Ms}$	×300
27	IKKa→ IKKi	2.3e-2	$\frac{1}{s}$	×15
28	IKKa + A20a→ IKKi + A20a	0.1	$\frac{1}{\mu Ms}$	
29	IKKa→ 0	1.3e-4	$\frac{1}{s}$	
30	IKKi→ 0	1.3e-4	$\frac{1}{s}$	
31	IKKa + IκBa→ IKKa∼IκBa	0.2	$\frac{1}{\mu Ms}$	
32	IKKa∼IκBa→ IKKa	0.1	$\frac{1}{s}$	
33	IκBa + NF–κB→ IκBa∼NF–κB	1.7e-1	$\frac{1}{\mu Ms}$	÷3
	IκBa + NF–κB← IκBa∼NF–κB	4.0e-5	$\frac{1}{s}$	
34	IKKa+IκBa∼NF–κB→ IKKa∼IκBa∼NF–κB	1.9	$\frac{1}{\mu Ms}$	×1.9
35	IKKa∼IκBa∼NF–κB →IKKa + NF–κB	2.5e-3	$\frac{1}{s}$	÷40
36	NF–κB→ 0	1.5e-3	$\frac{1}{s}$	÷3

37	NF–κB→ NF–κBn + NF–κB	3.75e-3	$\frac{1}{s}$	÷3
38	NF–κBn→ A20t + NF–κBn	5.0e-7	$\frac{1}{s}$	
39	A20t→ A20 + A20t	0.5	$\frac{1}{s}$	
40	A20→ 0	3.0e-4	$\frac{1}{s}$	
41	A20t→ 0	4.0e-4	$\frac{1}{s}$	
42	NF–κBn→ IκBat + NF–κBn	6.5e-7	$\frac{1}{s}$	×1.3
43	IκBat→ IκBa + IκBat	7.5e-1	$\frac{1}{s}$	×1.5
44	IκBat→ 0	1.0e-3	$\frac{1}{s}$	×2.5
45	IκBa→ 0	2.2e-3	$\frac{1}{s}$	
46	IκBa→ IκBan + IκBa	5e-3	$\frac{1}{s}$	
47	IκBan→ 0	2e-3	$\frac{1}{s}$	
48	IκBan→ IκBa + IκBan	8e-4	$\frac{1}{s}$	
49	IκBan + NF–κBn→ IκBan∼NF–κBn	0.5	$\frac{1}{\mu Ms}$	
	IκBan + NF–κBn← IκBan∼NF–κBn	2.0e-5	$\frac{1}{s}$	
50	IκBan∼NF–κBn→ 0	2.5e-2	$\frac{1}{s}$	
51	IκBan∼NF–κBn→ IκBa∼NF–κB + IκBan∼NF–κBn	1.0e-2	$\frac{1}{s}$	
52	NF–κBn→ IAPt + NF–κBn	7.0e-7	$\frac{1}{s}$	÷10
53	IAPt→ IAP + IAPt	6.5e-2	$\frac{1}{s}$	
54	IAPt→ 0	4e-4	$\frac{1}{s}$	
55	0→ IAP	2.7e-5	$\frac{\mu M}{s}$	×2.6
	0← IAP	1.9e-4	$\frac{1}{s}$	
56	NF–κBn→ FLIPt + NF–κBn	1.7e-4	$\frac{1}{s}$	÷2.5

57	FLIPt→ FLIP + FLIPt	2.9e-1	$\frac{1}{s}$	
58	FLIPt→ 0	4e-4	$\frac{1}{s}$	
59	0→ FLIP	1.7e-4	$\frac{\mu M}{s}$	×2
	0← FLIP	1.9e-4	$\frac{1}{s}$	
Caspase Module				
60	0→ C8	1.8e-5	$\frac{\mu M}{s}$	×1.3
	0← C8	8.5e-5	$\frac{1}{s}$	×1.3
61	0→ C3	3.0e-6	$\frac{\mu M}{s}$	×1.3
	0← C3	8.5e-5	$\frac{1}{s}$	×1.3
62	C8 + C2→ C8a + C2	7.5e-3	$\frac{1}{\mu M s}$	÷4
63	C8a + C3→ C8a + C3a	4.0e-2	$\frac{1}{\mu M s}$	÷2.5
64	C3a + C8→ C3a + C8a	4.0e-2	$\frac{1}{\mu M s}$	÷2.5
65	0→ Bid	2.8e-5	$\frac{\mu M}{s}$	
	0← Bid	1.7e-5	$\frac{1}{s}$	
66	C8a + Bid→ C8a∼Bid	4.0e-2	$\frac{1}{\mu M s}$	
67	C8a∼Bid→ tBid + C8a	4.0e-2	$\frac{1}{s}$	
68	tBid→ 0	5.0e-5	$\frac{1}{s}$	
69	C3a + IAP→ C3a∼IAP	5.0	$\frac{1}{\mu M s}$	
	C3a + IAP← C3a∼IAP	3.5e-3	$\frac{1}{s}$	
70	C3a∼IAP→ 0	2.9e-4	$\frac{1}{s}$	
71	C3a + IAP→ C3a	9.0	$\frac{1}{\mu M s}$	
72	C8a→ 0	7.7e-4	$\frac{1}{s}$	×8
73	C3a→ 0	9.7e-5	$\frac{1}{s}$	

Table 5.4: Reaction list.

Initial values

The following table summarizes the initial values for the (unstimulated) resting steady state. The initial concentration of TNF is the model input.

N	**Specie**	Initial Value [μM]
1	TNFR	2.4e-7
2	TNF	0
3	Cex	0
4	C0	0
5	RIP	6.7e-3
6	Czw0	0
7	C1	0
8	A20	4.9e-3
9	A20a	0
10	Czw1	0
11	Czw2	0
12	Czw3	0
13	Czw4	0
14	Czw5	0
15	Czw6	0
16	C2	0
17	C3a	0
18	FLIP	2.4
19	C2∼FLIP	0
20	IKKn	0.20
21	IKKa	0
22	IKKi	0
23	IκBα	5.8e-3
24	IKKα ∼IκBα	0

25	NF–κB	2.8e-03
26	IkBα ∼NF–κB	0.18
27	IKKa∼IκBa∼NF–κB	0
28	NF–κBn	2.4e-3
29	A20t	2.95e-6
30	IκBαt	1.5e-6
31	IκBan	9e-3
32	IκBan∼NF–κBn	4.3e-3
33	IAPt	4.2e-6
34	IAP	0.15
35	FLIPt	1e-3
36	C8	0.22
37	C3	0.035
38	C8a	0
39	Bid	1.7
40	C8a∼Bid	0
41	tBid	0
42	C3a∼IAP	0

Table 5.5: Initial values.

Lognormal Distribution Features

The log-normal distribution is the probability distribution of any random variable whose logarithm is normally (i.e. Gaussian) distributed. The differences to the normal distribution are fundamental: first, in the lognormal distribution random, independent effects are multiplicative, whereas they are additive in the Gaussian distribution. Second, the commonly used term average is in the lognormal distribution the geometric mean, e.g. the median, whereas it is the arithmetic mean in the normal distribution.

The probability density function (PDF) of the lognormal distribution is given by

$$f_{\mu,\sigma}(x) = \begin{cases} \dfrac{\exp(-(\ln x-\mu)^2/(2\sigma^2))}{x\sigma\sqrt{2\pi}} & (x>0) \\ 0 & (x\le 0), \end{cases}$$

and the cumulative distribution function (CDF) of the lognormal distribution is given by

$$f_{\mu,\sigma}(x) = \begin{cases} \dfrac{1}{2}+\dfrac{1}{2}\mathrm{erf}\left[\dfrac{\ln x-\mu}{\sigma\sqrt{2}}\right] & (x>0) \\ 0 & (x\le 0). \end{cases}$$

Herein, μ and σ denote the (lognormal) distribution parameters, and erf denotes the errorfunction.

Characteristics of the lognormal distribution

Table 5.6 lists some important characteristics and measures of the lognormal distribution.

Name	calculation
median	$\exp(\mu)$
geometric mean	$\mu_g = \exp(\mu)$
arithmetic mean	$\mathrm{E[X]} = \exp(\mu + \frac{\sigma^2}{2})$
variance	$\mathrm{Var}[X] = \left(\exp(\sigma^2 - 1)\right) \cdot \exp(2\mu + \sigma^2)$
variation coefficient	$\mathrm{VarK}[X] = \frac{\sqrt{\mathrm{Var(X)}}}{\mathrm{E[X]}} = \exp(\sigma^2 - 1)$
geometric deviation	$\sigma_g = \exp(\sigma)$

Table 5.6: Characteristics of the lognormal distribution.

Confidence intervals

The confidence intervals for the lognormal distribution are presented in Table 5.7 and depicted in Figure 5.1.

Confidence interval bounds	log space	geometric
3σ lower bound	$\mu - 3\sigma$	$\mu_\mathrm{g} \,/\, \sigma_\mathrm{g}^3$
2σ lower bound	$\mu - 2\sigma$	$\mu_\mathrm{g} \,/\, \sigma_\mathrm{g}^2$
1σ lower bound	$\mu - \sigma$	$\mu_\mathrm{g} \,/\, \sigma_\mathrm{g}$
1σ upper bound	$\mu + \sigma$	$\mu_\mathrm{g} \cdot \sigma_\mathrm{g}$
2σ upper bound	$\mu + 2\sigma$	$\mu_\mathrm{g} \cdot \sigma_\mathrm{g}^2$
3σ upper bound	$\mu + 3\sigma$	$\mu_\mathrm{g} \cdot \sigma_\mathrm{g}^3$

Table 5.7: Confidence Intervals for the lognormal distribution.

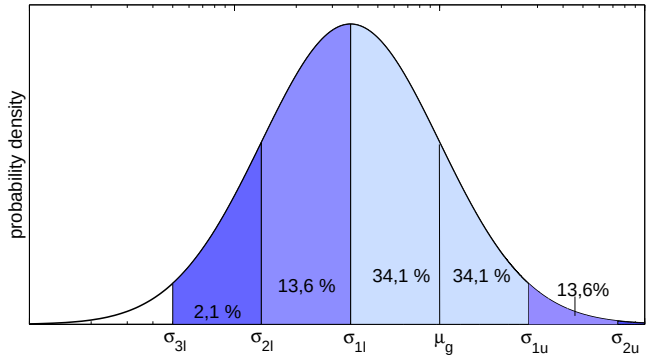

(a) Logarithmic scale.

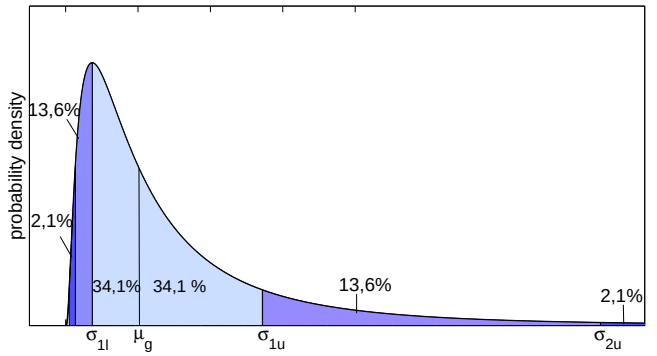

(b) Linear scale.

Figure 5.1: Confidence intervals and confidence bounds for the lognormal distribution.

Tests for lognormal distribution

Given a sample distribution of a population, the question arises whether the population is lognormally distributed or not. Due to the close relation to the normal distribution, normality tests can be applied. Normality tests check a given set of data for similarity to the normal distribution. The null hypothesis is that the data set is similar to the normal distribution, therefore a sufficiently small p–value indicates non-normal data. Several test algorithm exist, such as Kolmogorov-Smirnov (KS) test, Lilliefors test, and Anderson-Darling test.

The two-sample KS test is one of the most useful and general nonparametric method for comparing two samples, as it is sensitive to differences in both location and shape of the empirical cumulative distribution functions of the two samples. This test is used to check the hypothesis that a Kym–1 probe is lognormally distributed.